

TephAta - An online ~~data~~-collection of tephra data from the Atacama Desert

5 Niklas Leicher¹, Vincent Feldmar², Andrés Quezada Jara³, Paulina Vásquez Illanes³, Fernando Sepúlveda Vásquez³, Frank Wombacher¹, Markus Lagos⁴, Tanja Kramm², Gabriel González⁵, Klaudia Kuiper⁶, Christoph Breitkreuz⁷, Alberto Sáez⁸, Domingo Gimeno⁹, Lluís Cabrera⁸, Inés Rodríguez Araneda¹⁰, Bernd Wagner¹, Georg Bareth², Volker Wennrich¹

¹Institute of Geology and Mineralogy, University of Cologne, Cologne, 50672, Germany

²Institute of Geography, University of Cologne, Cologne, 50672, Germany

³Servicio Nacional de Geología y Minería (SERNAGEOMIN), Avenida Santa María 0104, Providencia, Santiago, Chile

10 ⁴Institute of Geosciences and Meteorology, University of Bonn, Bonn, 53115, Germany

⁵National Research Center for Integrated Natural Disaster Management, Departamento de Ciencias Geológicas, Universidad Católica del Norte, Antofagasta, Chile

⁶Department of Earth Sciences, Vrije Universiteit Amsterdam, Amsterdam, Netherlands

⁷Institut für Geologie und Paläontologie, Bernhard-von-Cotta-Str. 2, TU Bergakademie Freiberg, 09599 Freiberg, Germany

15 ⁸Geomodels Research Institute, Department Dinàmica de la Terra i de l'Oceà, Universitat de Barcelona, Martí Franques s/n, 08028 Barcelona, Spain

⁹Department de Mineralogia, Petrologia i Geologia Aplicada, Universitat de Barcelona, 08028 Barcelona, Spain

¹⁰Departamento de Obras Civiles y Geología, Universidad Católica de Temuco, Temuco, Chile

Correspondence to: Niklas Leicher (n.leicher@uni-koeln.de)

Abstract

Tephrostratigraphy and -chronology are powerful tools using volcanic ash (tephra) layers for establishing stratigraphic correlations and/or to obtain chronological information for different kinds of sedimentary archives. To develop tephrostratigraphic frameworks, ~~which ideally document a most complete spatial and temporal record of regional volcanic activity,~~ precise physical, geochemical and chronological characterization of tephra layers and their sampling site is needed. Based on these frameworks, newly discovered tephra layers can be linked to retrieve stratigraphic and chronological ~~information~~information and can contribute to reconstruct spatial and temporal records of regional volcanic activity. Tephrostratigraphic frameworks exist or are under construction for various regions of the world. However, for some regions ~~of the world~~ the potential of these methods is not exploited yet, One of these regions is the Atacama Desert of northern Chile, although being influenced by long-term and frequent volcanism and tephra deposition. ~~One of these regions is the Atacama Desert of northern Chile.~~ There, glass phase geochemical compositions of Pleistocene tephra layers ~~(volcanic glass)~~ were recently systematically investigated for their stratigraphy and chronology within the scope of the Collaborative Research Centre 'Earth – Evolution at the Dry Limit' (CRC-1211). ~~These analyses were accompanied~~In addition, a tephra database called TephAta by the was development developed of a tephra database called TephAta, which aims at providing a long-term basis for tephrostratigraphic and -chronological data of the Atacama Desert. TephAta allows digital documentation of the full variety of tephra-related datasets within one database and provides search functions to foster and simplify the continuous expansion of the regional framework following the FAIR (findability, accessibility, interoperability, and reusability) data principles. A first data compilation ~~of 106 tephra samples originate~~ from 91 tephra deposits is now available and will be continuously extended spatially and temporally. All data are accessible via the TephAta portal (<https://www.crc1211db.uni-koeln.de/tephata/>, last access: 16 March 2026) and data files described in this paper are available at <https://doi.org/10.60520/IEDA/114209> (Leicher N., 2026). TephAta does not only provide a stratigraphic and dating tool for paleoenvironmental or mapping studies, ~~but~~ it also helps to explore the integrity of the explosive volcanic history of the region along with the associated volcanic hazard and risk assessment.

45 1 Introduction

Volcanic ~~ashes (so-called tephra)~~ash deposits are intercalated within many ~~kinds-types~~ of sedimentary successions, ~~and serve as ideal chronological and stratigraphic marker horizons.~~ This makes them highly valuable as isochronous marker horizons for stratigraphic and chronological studies in fosters their use as targets for stratigraphic and chronological approaches, e.g., in geoscientific-geoscience and archaeological-archaeology studies (Lowe, 2011), ~~by tephrostratigraphy and -chronology.~~ The geochemical composition of volcanic glass is the most common and reliable parameter (Lowe et al., 2017) to construct tephrostratigraphic frameworks by correlating tephra layers, and to identify volcanic sources. Due to aeolian fractionation during volcanic ash dispersal, volcanic glass often remains as the major eruptive component, and its relative abundance increases with increasing distance ~~to from~~ the eruptive center. ~~Due to~~Because of its-the quenched nature, the glass's -character of glass, its geochemical composition closely resamples-reflects the composition of the magma at the time of eruption, acting as a distinctive and thus can be used as a characteristic fingerprint.

Tephrostratigraphy and -chronology ~~are is a~~ well-developed and frequently used techniques in many regions of the world including the Mediterranean (e.g., Sulpizio et al., 2003; Wulf et al., 2004; Giaccio et al., 2019; Leicher et al., 2021; Vakhrameeva et al., 2021), Northern Europe and the N-Atlantic (e.g., Griggs et al., 2014; Lowe et al., 2015; Abbott et al., 2018; Sáez et al., 2025), Central America (e.g., Kutterolf et al., 2016; Schindlbeck et al., 2018), New Zealand (e.g., Gehrels et al., 2006; Lowe et al., 2013; Hopkins et al., 2021) and eastern Asia (e.g., Sagawa et al., 2018; Albert et al., 2019; Portnyagin et al., 2020; Feng et al., 2022). Tephrochronological~~Tephrostratigraphic~~ databases exist for specific regions, e.g., for (northern)

Europe (TephraBase, Newton et al., 2007; Riede et al., 2011; RESET, Bronk Ramsey et al., 2015), the east African Rift (EarthD, Mana and Dimaggio, 2023), Alaska (GeoDIVA, Cameron et al., 2022), Kamchatka (TephraKam, Portnyagin et al., 2020), New Zealand (TephraNZ, Hopkins et al., 2021), southern Chile (BOOM!, Martínez Fontaine et al., 2023) or Antarctica (AnT, Kurbatov et al., 2014).

In some regions, however, ~~tephrochronology is not yet well established, despite a long history where of explosive volcanism that has produced frequent, widely distributed tephra layers with diverse geochemical compositions. has produced frequent and widely distributed tephra layers, tephrostratigraphy and chronology is not yet well established. Among these~~ Such a region is the western side of the Andes in Central South America, including the Atacama Desert. The Central Volcanic Zone of the Andes (14°-28° S; De Silva, 1989b) has a long volcanic activity (c. 240 Ma; Oliveros et al., 2018) and is ~~known-renowned~~ for major explosive eruptive events during the Neogene (c. 25-1 Ma, cf. Wörner et al., 2000; Burns et al., 2015; Van Zalinge et al., 2016). Geochemical variations specific to individual volcanoes and eruptions are driven not only by parental magma composition and the degree of crystallisation, but also by the geodynamic evolution of the Andes. Moreover, the geodynamic evolution of the Andes, and its The spatial and temporal differences in the thickness and composition of the crust, led to varying degrees of magma-crust interactions and thus ~~to good preconditions for the variable/additional~~ magmatic differentiation of individual eruptions (Kay et al., 2010; Brandmeier and Wörner, 2016; Burns and De Silva, 2023). ~~This is a prerequisite for determining eruption specific geochemical fingerprints that allow inter-site correlations of tephra layers and the construction of tephrostratigraphic frameworks.~~

The Atacama Deserts' long-term aridity, is thought to have initiated as early as ca. 25 Ma ago (Dunai et al., 2005; Evenstar et al., 2017) and sets with the low degree of erosion and weathering (e.g., Ritter et al., 2023) suitable climatic conditions for the preservation of volcanic deposits. Despite dominating easterly wind systems, ~~volcanic ash~~ tephra deposits can be found abundantly from the Andes to the Pacific coast (Marquardt et al., 2005; Vásquez and Sepúlveda, 2013; e.g., Breitkreuz et al., 2014). Tephra layers serve as crucial isochronous markers for dating sedimentary sequences within these arid environments, where other dateable materials are scarce and the temporal resolution often sediment records is often low. Thus, ~~The long-term aridity of the Atacama region, which is discussed to have started as early as ca. 25 Ma ago (Dunai et al., 2005; Evenstar et al., 2017), and the associated low degree of erosion (e.g., Ritter et al., 2023), ensured a good preservation of volcanic edifices and pyroclastic deposits in sedimentary archives. Nonetheless,~~ tephra layers of the Atacama region hitherto were mainly directly dated to constrain paleoenvironmental and tectonic processes (Sáez et al., 2012; Kirk-Lawlor et al., 2013; Jordan et al., 2014) or ~~during th~~ for use in extended geological mapping of the Chilean National Geology and Mining Survey (SERNAGEOMIN; e.g., Medina et al., 2012; Blanco and Tomlinson, 2013; Sepúlveda et al., 2014; Vásquez et al., 2018). Correlation of tephra layers by their glass geochemistry to establish local stratigraphic correlations is rare in the Atacama Desert Only very few tephra layers were investigated for their glass geochemical fingerprint to establish local stratigraphic correlations (Placzek et al., 2009; Breitkreuz et al., 2014; Tapia et al., 2015). In contrast, ~~rather~~ intensive research has been carried out on the magmatic evolution on the volcanoes of the Andes (e.g., De Silva, 1989a; Wörner et al., 2000; Kay et al., 2010; Mamani et al., 2010). Comprehensive results of this research including geochemical (whole-rock compositions and isotopes) and chronological data are made available within the Central Andes Geochemical and Geochronology database (<https://andes.gzg.geo.uni-goettingen.de/>). ~~This database provides basic, information concerning the volcanic sources of tephra layers, but the type of data (whole rock analyses) is~~

Whole-rock analyses, however, have been found to be less suitable for tephrochronological alignments due to site-dependent variations in their main components (variable relative abundances of glass, crystals and lithics) caused by aeolian fractionation, temporal eruptive variations and the influence of alteration (Tomlinson et al., 2012a; Lowe et al., 2017). less suitable to establish reliable correlations between tephra layers due to lateral variations in their crystal content (Tomlinson et al., 2012a; Lowe et al., 2017). Thus, A tephrostratigraphic framework based on glass geochemical compositions and geochronological data including the identification and detailed geochemical characterization of widespread marker horizons, which can be used

105 ~~for stratigraphic correlations and the transfer of ages between equivalent tephra layers, however,~~ is currently missing at the western side of the Andes.

The Collaborative Research Centre “Earth – Evolution at the Dry Limit” (CRC-1211) aims at disentangling how the shaping of land-surfaces by past episodes of wetter climate coevolved with the evolution of life in arid environments (Dunai et al., 2020). The main working area of the CRC is the Atacama Desert in Chile (Fig. 1a). For ~~its-this~~ multidisciplinary endeavor, 110 ~~establishing~~ chronological control ~~on-of~~ the sedimentary climate archives and ~~determination-determining the timing of dates~~ and rates of surface processes are of fundamental importance. ~~The inherent lack of dateable material in the hyperarid Atacama limits alternative chronological methods. Tephra layers represent a promising alternative, appearing across diverse sedimentary archives such as alluvial, fluvial, lacustrine, salar, and playa deposits. Furthermore, the scarcity of dateable material in the extreme desert environment of the Atacama Desert limits the chronological information provided by other dating methods.~~ 115 ~~One promising dating target are tephra layers, which are found in various sedimentary archives in the desert, including alluvial and fluvial deposits, lacustrine, salars and playa deposits~~ (Sáez et al., 2012; Jordan et al., 2014; Vásquez et al., 2018; Medialdea et al., 2020; Ritter et al., 2022; Wennrich et al., 2025). ~~Within the CRC1211, tephrochronology was used systematically to establish a time-stratigraphic framework for the Atacama Desert. Within the CRC1211, therefore, volcanic glass shards of tephra layers in the Atacama Desert were for the first time systematically investigated geochemically for tephrostratigraphic and tephrochronological purposes.~~ 120 ~~The~~ ~~se-~~ ~~obtained~~ ~~data~~ ~~is~~ ~~are~~ stored in ~~the~~ ~~a~~ newly developed regionally focused tephra database, TephAta. ~~TephAta can store a wide variety of tephra metadata, from field and lab context to physical, chemical and chronological characteristics. TephAta is designed to combine the vast variety of datasets that can be obtained for tephra samples ranging from field and lab metadata to morphological, geochemical, stratigraphic, and chronological datasets.~~ Storing the data in the dedicated TephAta database will ~~facilitate to facilitate~~ ~~focus on~~ the development of a regional tephrostratigraphic 125 framework for the Atacama Desert. TephAta provides easy access to complex information that normally is distributed in several media (publications, private or public databases), hence fostering FAIR (findable, accessible, interoperable and reusable) data principals (Wilkinson et al., 2016). The design of TephAta is also meant to provide user friendly integration of suitable parts of the dataset (e.g. geochemical data) in global databases such as GEOROC (<https://georoc.eu/>) or the tephra-data-optimized EARTHCHEM (<https://www.earthchem.org/>) repository. This paper introduces the TephAta database and 130 illustrates its usefulness by the presentation and discussion of an exemplary dataset obtained on widely distributed tephra deposits of Mid Pleistocene age from the central Atacama Desert.

2 The Central Volcanic Zone of the Andes

The subduction of the Farallon plate underneath the west coast of South America has caused continental arc volcanism within the Central Andes since Triassic times (Oliveros et al., 2018). The volcanic arc is characterized by low-flux, steady state 135 andesitic magmatism and the construction of composite volcanoes (Burns et al., 2015). Starting about 25 Ma ago, an increase of the subduction rate and a shift in the subduction geometry of the Nazca Plate caused a eastward migration of the arc and associated crustal shortening and thickening (Allmendinger et al., 1997). This change is correlated with a shift to a high-flux, flare-up arc magmatism, which resulted in the production and eruption of large volumes of silicic “crustal” magmas (Wörner et al., 2018; Burns and De Silva, 2023). Ignimbrite volcanism is supposed to be not contemporaneous within the Central 140 Volcanic Zone, indicating a north-south gradient towards younger major eruptive events (De Silva, 1989b; De Silva and Kay, 2018). The oldest ignimbrite deposits are incorporated within the Altos de Pica Formation (22-25 Ma; Jordan et al., 2014), the Oxaya Formation (19-23 Ma; Wörner et al., 2002; Van Zalinge et al., 2016) and the El Diablo Formations (11-16 Ma; Jordan et al., 2014). Between 10 and 1 Ma, magmatic fluxes strongly increased and numerous voluminous ignimbrites were erupted in pulses peaking at ca. 8.4 Ma, 5.5 Ma and 4.0 Ma (De Silva, 1989b; Sáez et al., 1999; Kay et al., 2010; Salisbury et al., 2011; 145 Burns and De Silva, 2023). One of the most prominent surface morphologies of these ignimbrite deposits is the Altiplano-Puna Volcanic Complex (APVC) between 21 and 24°S (De Silva, 1989a). Subsequently, the high-flux volcanic activity waned

and the construction of composite volcanoes and small-volume lava domes indicate the return to steady-state conditions (Burns and De Silva, 2023).

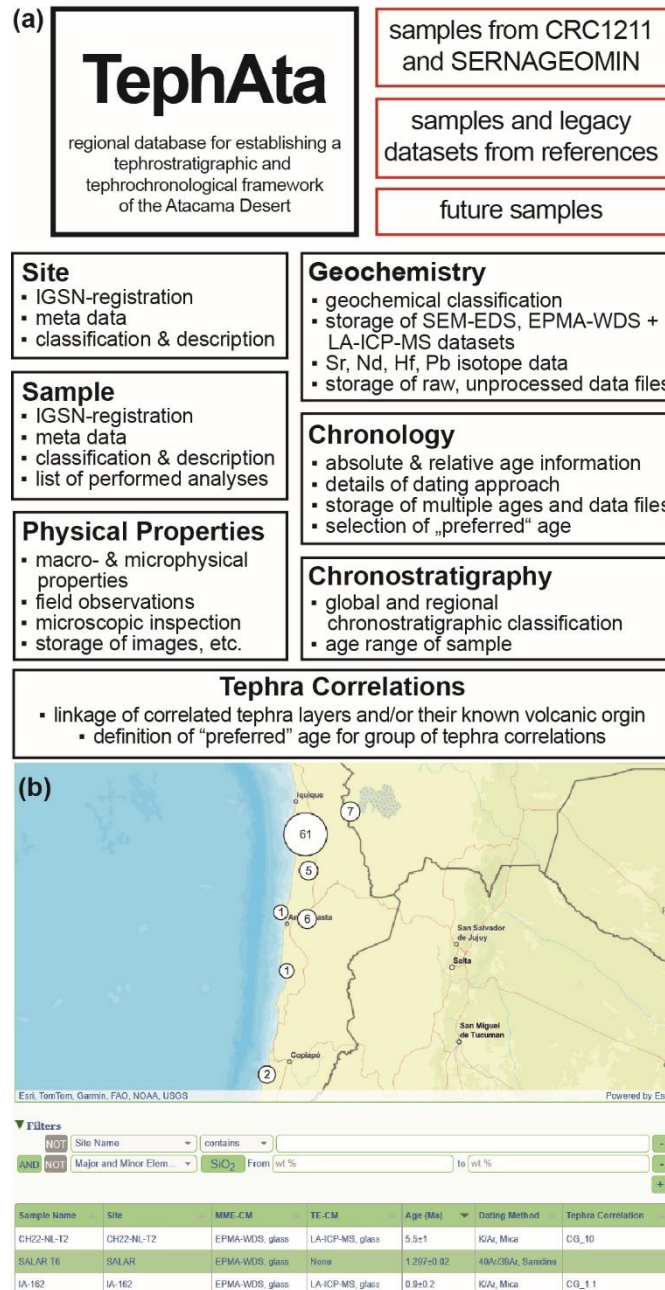


Figure 1: S (a) Structure of TephAta~~TA~~ with its seven categories and different sources for data. (b) An example employing the sample filter function of TephAta~~TA~~ showing the filtered samples on a map and listing them below (CRC1211-TephAta~~TA~~TephAta, 2025).

3 Database structure, samples, and analytical data

150 3.1 Database Structure

TephAta is hosted within the CRC1211 database (<https://www.crc1211db.uni-koeln.de>) and is focused entirely on storing and displaying information without data analysis by respective algorithms. In the backend, TephAta uses a relational database using MariaDB as data management system, communicating with a basic PHP instance hosted by the ITCC on virtual machines, while the frontend is handled by standard web technologies, with some display libraries (such as Tabulator or HighCharts) providing JavaScript interactivity. TephAta is designed to store site and sample metadata of tephra samples in combination with respective analytical datasets. The requested data structure is adapted to the global tephra community

guidelines for data acquisition and reporting outlined in Wallace et al. (2022). Data can origin from new investigations, but also from published work.

TephAta is organized into seven data categories: site, sample, physical properties, geochemistry, ~~morphology~~, chronology, chronostratigraphy, and equivalent tephra correlations (Fig. 1a). A general introduction of the data stored in the different categories is given below and a full list and description of all input fields and upload functions is given in Supplementary Table +Material.

The category “site” allows the documentation of sample location details including information about the site name ~~(title)~~, a general (log-) description, geographic position, physical habitus, and spatial context of an investigated location. The site category lists and links all samples taken from the same archive.

The section “sample” provides information when, how and by whom a sample from a specific site was taken. Further details about the sample type and material, its position within a site and the observed depositional processes can be defined. Information about sub- or split-samples and related (laboratory) labels can be listed together with the availability and accessibility of material and data. Specific analyses that were carried out can be indicated in an overview list.

The category “physical properties” collects field and microscopic observations. These include descriptions of the macrophysical properties of the stratigraphic layer (thickness, color, sedimentological structures, components), and its microphysical characteristics such as glass fragment morphology, mineral assemblages, or degree of alteration. Field sketches, images or notes and microscopic images can also be integrated.

The “geochemistry” category facilitates the classification data input allows definition of the volcanic rock types of a specific sample based on thusing the total alkali vs silica (TAS) classification (Le Bas et al., 1986). Geochemical datasets of major (>1 wt.%), minor (1-0.1 wt.%) and trace (<0.1 wt.%) element data, but also Sr, Nd, Pb isotope data can be archived. Unprocessed raw data, instrument log files and laboratory protocol data of geochemical analyses can be stored as supplementary files.

~~The category “morphology” collects morphological and sample component observations from the field and from microscopic inspection. These include descriptions of the macrophysical properties of the stratigraphic layer where a specific sample was taken from (thickness, color, sedimentological structures, components), but also its microphysical properties (glass fragment morphology, mineral assemblages, degree of alteration). Field sketches, images or notes and microscopic images can also be integrated.~~

The “~~chronology~~chronology” category collects age information related to a specific sample. Details on the applied dating technique(s) can be entered along with information about the dated material and specific age information (uncertainties, type of age calculation, xenocryst presence). Full analytical datasets including laboratory details as well as unprocessed and processed data-files (e.g., single crystal dating results) can be stored as supplementary files. For samples with Mmultiple age determinations (e.g., by different dating techniques), users can ~~be entered for a single sample including the definition of~~ adesignate a “best age”, which will be assigned to represent as the most reliable age estimate in the sample overview.

Within the data category “chronostratigraphy” a specific sample can be categorized by its general (e.g. Erathem, Stage, etc.) and regional stratigraphic classifications. When available, this information is used to define minimum and maximum age constraints. If (chrono)stratigraphic information allows, a minimum and a maximum age can be defined.

For samples ~~for which~~ could be correlated with otheran equivalent tephra samples or a specific volcanic eruption ~~is identified and confirmed~~ by tephrostratigraphic means, a link between samples can be documented within ~~the~~ “tephra correlationequivalent” category. Equivalent gGroups of correlated tephra can be further defined by a common name and their most reliable age. In case a tephra layer can be traced back to ~~its a~~ specific volcanic origin, both the source volcano and eruption can be linked to the equivalent group, respective correlation.

All ~~the aforementioned~~ data is entered via the TephAta web interface (<https://www.crc1211db.uni-koeln.de/tephata>) using guided input forms, including unified predefined lists, as well as free-~~text~~ fields for the input of individual data items. Geochemical data can be uploaded (and downloaded) by-using template data sheets provided on the website. The template

200 files ~~combine-integrate~~ sample and instrument metadata (e.g., sample IDs and types, related references, applied analytical protocols and instrument) with ~~respective~~ results ~~from~~ of standards and samples, ~~ensuring-to-ensure~~ transparent documentation for interoperability and data reuse.

-For all categories additional data files (e.g., raw data and detailed instrument settings, field, and sample photo documentation) can be uploaded as zip-files. Datasets stored within TephAta can be continuously extended, as additional analyses ~~and methods~~ become available. ~~-If no IGSN (International Generic Sample Number) was assigned to a site or sample before registration within TephAta, a new IGSN will be minted and connected with the internal metadata upon data submission in TephAta by the GFZ Potsdam Data Services. A new IGSN will then be associated with the TephAta URL, providing a link to the full metadata released within the database. Existing IGSN can be linked to a sample during data submission. Based on the site and sample metadata, TephAta requests IGSNs (International Generic Sample Number), to enable a unique identification of a site and a sample.~~ The IGSN ~~enables a unique identification of a site and a sample including also allows~~ documentation outside TephAta and provides a connection to other databases. Data exchange to other global databases is also fostered by the structures of file templates, which are organized to match the needs of the global tephra-data repository EarthChem (<https://www.earthchem.org/>; Kuehn et al., 2023).

Datasets stored within TephAta can be accessed through the categories: “sites” and “samples”. ~~All data associated with a given sample or site are presented on a dedicated page that compiles and displays all shared entries.~~ The sample list is linked to a map tool, which allows exploring entries within a specific ~~geographic areas~~ (Fig. 1b). The sample list can be ~~adapted-refined using~~by combinable filters, ~~including for~~ specific site, sample and ~~equivalent names~~group of tephra correlations ~~names~~ (site name, sample name, lab ID, ~~IGSN, equivalent title~~name of group of tephra correlations). Users can also filter by ~~;~~ the type of site (e.g., only alluvial fans), ~~and~~ geochemical properties (TAS-classification, range of specific major, minor and/or trace element concentrations) ~~and~~. ~~Samples can be also filtered for their~~ ~~chrono~~stratigraphic (series) and chronological (age range) values.

-Furthermore, users can select up to 15 samples to create compositional x-y plots. An overview of established tephra correlations is given by the ~~“equivalent group~~tephra correlations” list. ~~These functions are designed to facilitate the identification of potential tephra correlations, providing the basis for detailed testing and subsequent establishment of tephrochronological frameworks.~~

~~These functions shall foster the use of the database to identify potential equivalent tephra layers and thus provide the basis for detailed testing and subsequent establishment of tephrostratigraphic and chronological correlations.~~

Table 1: Overview table listing all sites and samples included within [TephATA-TephAta](#) along with information about their type of site, proposed age and dating details (if available, age and age uncertainty, dating method, dated mineral, dating laboratory, mineral standard and decay constant applied, type of age and reference of age). Further it is listed if the tephra was previously known and the sample was provided or (re-)sampled within the activities of the CRC1211, more details about the origin of samples are given within TephAta database. Sample AD-85 was provided by J. Quade (University of Arizona, [USA](#)) and sample TJ09-PdT-1 was provided by T. Jordan (Cornell University, [USA](#)).

235 References are: 8= Blanco and Tomlinson (2013) 16= Rodríguez et al. (2015)
1=Breitkreuz et al. (2014) 9= Medina et al. (2012) 17= Horn (1991)
2= Placzek et al. (2009) 245 10=Escibano et al. (2013) 18=Wörner et al. (2000)
3 = Sáez et al. (2012) 11= Marinovic et al. (1995) 19= Medialdea et al. (2020)
4= Ritter et al. (2018) 12= Carrizo et al. (2008) 255 20= Fornari et al. (2001)
240 5= this study 13=Vásquez et al. (2018) 21= Fritz et al. (2004)
6= Gardeweg and Sellés (2013) 14=Vásquez and Sepúlveda (2013) 22= Sepúlveda et al. (2023)
7= Astudillo et al. (2017) 250 15= Sepúlveda et al. (2014) 23= May et al. (2020)

site	sample	2nd sample name / resampled equivalent	type of site	age (Ma)	age uncertainty (Ma)	dating method	dated mineral	dating laboratory	Ar-Ar mineral standard, decay constant	type of age	reference	sample source	known or new sample
10-3-5-1	10-3-5-1	L-10	alluvial fan	not dated	not dated	N/A	N/A	N/A	N/A	N/A	1	reference	known
19MEJ9	19MEJ09	-	alluvial fan	not dated	not dated	N/A	N/A	N/A	N/A	N/A	-	CRC	new
AD-1	AD-1	-	alluvial fan	0.750	0.060	⁴⁰ Ar/ ³⁹ Ar	biotite	Sernageomin	FC; Steiger & Jäger (1977)	plateau	2	reference	known
ARC	ARC1	-	alluvial fan	not dated	not dated	N/A	N/A	N/A	N/A	N/A	3	reference	known
Asche 4 / PAG-T4	PAG-T4	PAG TEPH RA 4	channel	0.980	0.040	U/Pb	zircon	University of Frankfurt	N/A	TuffZirc	4	CRC	new
Asche 4 / PAG-T4	PAG-T4	PAG TEPH RA 4	channel	0.301	0.007	⁴⁰ Ar/ ³⁹ Ar	biotite	University of Amsterdam	FC; Min et al. (2000)	weighted mean total fusion	5	CRC	new
ATA19-023 / CR-006	ATA19-023	CR-006A	ignimbrite deposits	equivalent dated	equivalent dated	N/A	N/A	N/A	N/A	N/A	-	CRC	known
ATA19-023 / CR-006	CR-006A	ATA19-023	ignimbrite deposits	0.280	0.014	⁴⁰ Ar/ ³⁹ Ar	biotite	Sernageomin	FC; Steiger & Jäger (1977)	plateau	6	reference	known
AVN-002	AVN-002d	-	alluvial fan	0.740	0.080	⁴⁰ Ar/ ³⁹ Ar	biotite	Sernageomin	FC; Steiger & Jäger (1977)	plateau	7	SERNAGEOMIN	known
C2-TEP-04/IT93	C2-TEP-04	IT-93	channel	equivalent dated	equivalent dated	N/A	N/A	N/A	N/A	N/A	-	CRC	known
C2-TEP-04/IT93	IT-93	C2-TEP-04	channel	0.170	0.040	⁴⁰ Ar/ ³⁹ Ar	biotite	Sernageomin	FC; Steiger & Jäger (1977)	plateau	8	reference	known
C2-TEP-05/IT307	C2-TEP-05	IT-307	channel	equivalent dated	equivalent dated	N/A	N/A	N/A	N/A	N/A	-	CRC	known
C2-TEP-05/IT307	IT-307	C2-TEP-05	channel	0.400	0.100	K-Ar	biotite	Sernageomin	Steiger & Jäger (1977)	N/A	8	reference	known

site	sample	2nd sample name / resampled equivalent	type of site	age (Ma)	age uncertainty (Ma)	dating method	dated mineral	dating laboratory	Ar-Ar mineral standard, decay constant	type of age	reference	sample source	known or new sample
CC157 / L8 / 2/3/5/2	2/3/5/2	CC-157 // L8	alluvial fan	equivalent dated	equivalent dated	N/A	N/A	N/A	N/A	N/A	1	reference	known
CC157 / L8 / 2/3/5/2	CC-157	2/3/5/2 // L8	alluvial fan	0.230	0.130	⁴⁰ Ar/ ³⁹ Ar	biotite	Sernageomin	FC; Steiger & Jäger (1977)	inverse isochron	9	reference	known
CH17-001 (AD-85)	AD-85	CH17-001	channel	not dated	not dated	N/A	N/A	N/A	N/A	N/A	-	J. Quade	new
CH17-001 (AD-85)	CH17-001	AD-85	channel	not dated	not dated	N/A	N/A	N/A	N/A	N/A	-	CRC	new
CH18-T1-4	CH18-T1	-	alluvial fan	not dated	not dated	N/A	N/A	N/A	N/A	N/A	-	CRC	new
CH18-T1-4	CH18-T2	-	alluvial fan	not dated	not dated	N/A	N/A	N/A	N/A	N/A	-	CRC	new
CH18-T1-4	CH18-T3	-	alluvial fan	not dated	not dated	N/A	N/A	N/A	N/A	N/A	-	CRC	new
CH18-T1-4	CH18-T4	-	alluvial fan	not dated	not dated	N/A	N/A	N/A	N/A	N/A	-	CRC	new
CH18-T5	CH18-T5	-	alluvial fan	not dated	not dated	N/A	N/A	N/A	N/A	N/A	-	CRC	new
CH22-NL-T1	CH22-NL-T1	TPM-094	alluvial fan	3.900	0.800	⁴⁰ Ar/ ³⁹ Ar	biotite	Sernageomin	FC; Steiger & Jäger (1977)	combined isochron n=2	10	CRC	known
CH22-NL-T2	CH22-NL-T2	MAB-663	alluvial fan	5.500	1.000	K-Ar	biotite	Sernageomin	N/A	N/A	11	CRC	known
CH22-NL-T3	CH22-NL-T3-1	-	alluvial fan	not dated	not dated	N/A	N/A	N/A	N/A	N/A	-	CRC	known
CH22-NL-T3	CH22-NL-T3-2	-	alluvial fan	not dated	not dated	N/A	N/A	N/A	N/A	N/A	-	CRC	known
CHU / AN1	CHU Tephra	AN1	fault scarp	equivalent dated	equivalent dated	N/A	N/A	N/A	N/A	N/A	-	SERNAG EOMIN	known
CHU / AN1	AN-1	CHU-Tephra	fault scarp	0.310	0.190	⁴⁰ Ar/ ³⁹ Ar	biotite	Sernageomin	N/A	plateau	12	reference	known
CHU-1	CHU-1	-	channel	not dated	not dated	not dated	N/A	N/A	N/A	N/A	-	SERNAG EOMIN	known
CHU-2	CHU-2	-	badlands	not dated	not dated	not dated	N/A	N/A	N/A	N/A	-	SERNAG EOMIN	known
CON-1	CON-1	-	channel	0.181	0.056	⁴⁰ Ar/ ³⁹ Ar	biotite	GEOMAR Kiel	TCR-2, unknown	plateau	3	reference	known
CTFON-4	CTFON-4	-	marine deposits	not dated	not dated	not dated	N/A	N/A	N/A	N/A	-	CRC	known
EL Rincon	19MEJ10	-	marine deposits	not dated	not dated	N/A	N/A	N/A	N/A	N/A	-	CRC	new
EL Rincon	23MEJ1	-	marine deposits	not dated	not dated	N/A	N/A	N/A	N/A	N/A	-	CRC	new
ESQ-1	ESQ-1	-	channel	0.151	0.033	⁴⁰ Ar/ ³⁹ Ar	biotite	GEOMAR Kiel	TCR-2	plateau	3	reference	known
GSQ-027	GSQ-027d	-	terrace	0.255	0.017	⁴⁰ Ar/ ³⁹ Ar	biotite	Sernageomin	FC; Steiger & Jäger (1977)	plateau	13	SERNAG EOMIN	known
GSQ-08	GSQ-08d	-	terrace	0.300	0.020	⁴⁰ Ar/ ³⁹ Ar	biotite	Sernageomin	FC; Steiger & Jäger (1977)	plateau	13	SERNAG EOMIN	known
GSQ-106d	GSQ-106d	-	alluvial fan	0.329	0.029	⁴⁰ Ar/ ³⁹ Ar	biotite	Sernageomin	FC; Steiger & Jäger (1977)	plateau	13	SERNAG EOMIN	known
GSQ-158	GSQ-158d	-	alluvial fan	0.340	0.021	⁴⁰ Ar/ ³⁹ Ar	biotite	Sernageomin	FC; Steiger & Jäger (1977)	plateau	13	SERNAG EOMIN	known
GSQ-53	GSQ-53d	-	alluvial fan	0.325	0.048	⁴⁰ Ar/ ³⁹ Ar	biotite	Sernageomin	FC; Steiger & Jäger (1977)	plateau	13	SERNAG EOMIN	known

site	sample	2nd sample name / resampled equivalent	type of site	age (Ma)	age uncertainty (Ma)	dating method	dated mineral	dating laboratory	Ar-Ar mineral standard, decay constant	type of age	reference	sample source	known or new sample
GSV-132	GSV-132d	-	fault scarp	0.140	0.057	$^{40}\text{Ar}/^{39}\text{Ar}$	biotite	Sernageomin	FC; Steiger & Jäger (1977)	plateau	13	SERNAG EOMIN	known
HU14/008 (IS-155)	HU14/008	IS-155	claypan	equivalent dated	equivalent dated	N/A	N/A	N/A	N/A	N/A	-	CRC	known
HU14/008 (IS-155)	IS-155	HU14/008	claypan	22.9	0.3	$^{40}\text{Ar}/^{39}\text{Ar}$	biotite	Sernageomin	FC; Steiger & Jäger (1977)	plateau	14	SERNAG EOMIN	known
HU17-014	HU17-014	-	channel	not dated	not dated	N/A	N/A	N/A	N/A	N/A	-	CRC	new
HU18/001/002	HU18/001	-	channel	not dated	not dated	N/A	N/A	N/A	N/A	N/A	-	CRC	new
HU18/001/002	HU18/002	-	channel	not dated	not dated	N/A	N/A	N/A	N/A	N/A	-	CRC	new
HU18-003 (IV-190)	HU18/003	IV-190	channel	equivalent dated	equivalent dated	N/A	N/A	N/A	N/A	N/A	-	CRC	known
HU18-003 (IV-190)	IV-190	HU18/003	channel	0.620	0.040	$^{40}\text{Ar}/^{39}\text{Ar}$	biotite	Sernageomin	FC; Steiger & Jäger (1977)	plateau	14	SERNAG EOMIN	known
HU18-008 (IV-189)	HU18/008	IV-189	channel	equivalent dated	equivalent dated	N/A	N/A	N/A	N/A	N/A	-	CRC	known
HU18-008 (IV-189)	IV-189	HU18-008	channel	2.06	0.12	$^{40}\text{Ar}/^{39}\text{Ar}$	biotite	Sernageomin	FC; Steiger & Jäger (1977)	inverse isochron	14	reference	known
IA-05	IA-05	-	alluvial fan	0.40	0.20	K-Ar	biotite	Sernageomin	FC; Steiger & Jäger (1977)	combined K-Ar n=2	15	SERNAG EOMIN	known
IA-105	IA-105	-	alluvial fan	0.314	0.012	$^{40}\text{Ar}/^{39}\text{Ar}$	biotite	Sernageomin	FC; Steiger & Jäger (1977)	plateau	15	SERNAG EOMIN	known
IA-11	IA-11	-	channel	0.430	0.040	$^{40}\text{Ar}/^{39}\text{Ar}$	biotite	Sernageomin	FC; Steiger & Jäger (1977)	inverse isochron	15	SERNAG EOMIN	known
IA-120	IA-120	-	alluvial fan	0.300	0.200	K-Ar	biotite	Sernageomin	FC; Steiger & Jäger (1977)	combined K-Ar n=2	15	SERNAG EOMIN	known
IA-137	IA-137	-	channel	0.700	0.400	K-Ar	biotite	Sernageomin	FC; Steiger & Jäger (1977)	N/A	15	SERNAG EOMIN	known
IA-162	IA-162	-	alluvial fan	0.900	0.200	K-Ar	biotite	Sernageomin	FC; Steiger & Jäger (1977)	combined K-Ar n=2	15	SERNAG EOMIN	known
CH22-NL-T46	CH22-NL-T46	IA-270?	hillslope	equivalent dated	equivalent dated	N/A	N/A	N/A	N/A	N/A	-	CRC	known
IA-270	IA-270	CH22-NL-T46?	alluvial fan	0.410	0.030	$^{40}\text{Ar}/^{39}\text{Ar}$	biotite	Sernageomin	FC; Steiger & Jäger (1977)	plateau	15	SERNAG EOMIN	known
IA-95	IA-95	-	alluvial fan	0.500	0.300	K-Ar	biotite	Sernageomin	FC; Steiger & Jäger (1977)	N/A	15	SERNAG EOMIN	known
IA-97	IA-97	-	alluvial fan	0.600	0.300	K-Ar	biotite	Sernageomin	FC; Steiger & Jäger (1977)	combined K-Ar n=2	15	SERNAG EOMIN	known
IQ18-001	IQ18-001	-	alluvial fan	not dated	not dated	N/A	N/A	N/A	N/A	N/A	-	CRC	known

site	sample	2nd sample name / resampled equivalent	type of site	age (Ma)	age uncertainty (Ma)	dating method	dated mineral	dating laboratory	Ar-Ar mineral standard, decay constant	type of age	reference	sample source	known or new sample
IQ18-002 (CMI13.3)	CMI13.3	IQ18-002	alluvial fan	0.700	0.110	⁴⁰ Ar/ ³⁹ Ar	biotite	Sernageomin	FC; Steiger & Jäger (1977)	plateau	14	SERNAG EOMIN	known
IQ18-002 (CMI13.3)	IQ18-002	CMI13.3	alluvial fan	equivalent dated	equivalent dated	N/A	N/A	N/A	N/A	N/A	-	CRC	known
IR22-01	IR22-001	-	ignimbrite deposits	not dated	not dated	N/A	N/A	N/A	N/A	N/A	-	CRC	known
IR22-02	IR22-002	-	ignimbrite deposits	not dated	not dated	N/A	N/A	N/A	N/A	N/A	-	CRC	known
IRRU-13	IRRU-13	-	flank of volcano	not dated	not dated	N/A	N/A	N/A	N/A	N/A	16	reference	known
IRRU-46a	IRRU-46a	-	flank of volcano	0.258	0.049	⁴⁰ Ar/ ³⁹ Ar	biotite	Oregon State University	FC	inverse isochron	16	reference	known
IRU-15	IRU-15	-	ignimbrite deposits	0.320	0.250	K-Ar	biotite	NERC	N/A	plateau	17, 8	reference	known
IRU-1a	IRU-1a	-	flank of volcano	0.181	0.009	⁴⁰ Ar/ ³⁹ Ar	biotite	University of Amsterdam	FC; Min et al. (2000)	weighted mean total fusion	5, 17, 18	reference	known
PAG	PAG17 ID14	-	claypan	not dated	not dated	N/A	N/A	N/A	N/A	N/A	-	CRC	new
PAG	PAG17 ID24	-	claypan	not dated	not dated	N/A	N/A	N/A	N/A	N/A	-	CRC	new
PAG	PAG17 ID4	-	claypan	not dated	not dated	N/A	N/A	N/A	N/A	N/A	-	CRC	new
PAG	PAG17 ID54	-	claypan	not dated	not dated	N/A	N/A	N/A	N/A	N/A	-	CRC	new
PAG T-1-2	PAG-T1	PAG TEPHRA 1	claypan	not dated	not dated	N/A	N/A	N/A	N/A	N/A	-	CRC	new
PAG T-1-2	PAG-T2	PAG TEPHRA 2	channel	not dated	not dated	N/A	N/A	N/A	N/A	N/A	-	CRC	new
PAG17.2-008	PAG17.2-008	-	channel	not dated	not dated	N/A	N/A	N/A	N/A	N/A	-	CRC	new
PAG17/001	PAG17/001	-	alluvial fan	not dated	not dated	N/A	N/A	N/A	N/A	N/A	-	CRC	new
PAG17/006	PAG17/006	-	channel	not dated	not dated	N/A	N/A	N/A	N/A	N/A	-	CRC	new
PAG17/027	PAG17/027	-	channel	not dated	not dated	N/A	N/A	N/A	N/A	N/A	-	CRC	new
PAG18/001	PAG18/001	-	channel	not dated	not dated	N/A	N/A	N/A	N/A	N/A	-	CRC	new
PAG18/002	PAG18/002	-	alluvial fan	not dated	not dated	N/A	N/A	N/A	N/A	N/A	-	CRC	new
PAG18/003	PAG18/003	-	alluvial fan	not dated	not dated	N/A	N/A	N/A	N/A	N/A	-	CRC	new
PAG18/008	PAG18/008	-	channel	not dated	not dated	N/A	N/A	N/A	N/A	N/A	-	CRC	new
POR 3	POR 3	-	flank of volcano	0.290	0.450/0.290	K-Ar	feldspar	NERC	Steiger and Jager, 1977	No reliable ages	17, 18	reference	known
POR 3	POR 3	-	flank of volcano	0.150	0.200/0.150	K-Ar	biotite	NERC	Steiger and Jager, 1977	No reliable ages	17, 18	reference	known
QP	QP1	-	channel	not dated	not dated	N/A	N/A	N/A	N/A	N/A	3	reference	known
QP	QP4	-	channel	not dated	not dated	N/A	N/A	N/A	N/A	N/A	3	reference	known
Quebrada Ancha	Tephra RB	-	channel	not dated	not dated	N/A	N/A	N/A	N/A	N/A	-	CRC	new
Quebrada Tiburón - Section A	TIB4-TEPH1	-	marine deposits	not dated	not dated	N/A	N/A	N/A	N/A	N/A	-	CRC	new

site	sample	2nd sample name / resampled equivalent	type of site	age (Ma)	age uncertainty (Ma)	dating method	dated mineral	dating laboratory	Ar-Ar mineral standard, decay constant	type of age	reference	sample source	known or new sample
Quebrada Tiburón - Section A	TIB4-F2	-	marine deposits	not dated	not dated	N/A	N/A	N/A	N/A	N/A		CRC	new
RL North	Tephra RL N	-	alluvial fan	not dated	not dated	N/A	N/A		N/A	N/A	-	CRC	new
SALAR	SG17/001	SALAR T6	hillslope	equivalent dated	equivalent dated	N/A	N/A	N/A	N/A	N/A	-	CRC	new
SALAR	SG17/002	SALAR T4	hillslope	equivalent dated	equivalent dated	N/A	N/A	N/A	N/A	N/A	-	CRC	new
SALAR	SG17/003	SALAR T2	hillslope	equivalent dated	equivalent dated	N/A	N/A	N/A	N/A	N/A	-	CRC	new
SALAR	SALAR T6	SG17/001	hillslope	1.297	0.018	⁴⁰ Ar/ ³⁹ Ar	sanidine	University of Amsterdam	FC; Min et al., 2000	weighted mean total fusion	19	CRC	new
SALAR	SALAR T6	-	hillslope	0.098	0.015	indirect - sediment OSL dating + absolute	N/A	University of Cologne	N/A	AGE-MODE L	19	CRC	new
SALAR	SALAR T5	-	hillslope	0.084	0.008	indirect - sediment OSL dating	N/A	University of Cologne	N/A	AGE-MODE L	19	CRC	new
SALAR	SALAR T4	SG17/002	hillslope	0.083	0.009	indirect - sediment OSL dating	N/A	University of Cologne	N/A	AGE-MODE L	19	CRC	new
SALAR	SALAR T3	-	hillslope	0.072	0.008	indirect - sediment OSL dating	N/A	University of Cologne	N/A	AGE-MODE L	19	CRC	new
SALAR	SALAR T2	SG17/003	hillslope	0.071	0.007	indirect - sediment OSL dating	N/A	University of Cologne	N/A	AGE-MODE L	19	CRC	new
SALAR	SALAR T1	-	hillslope	0.068	0.008	indirect - sediment OSL dating	N/A	University of Cologne	N/A	AGE-MODE L	19	CRC	new
Salar de Uyuni - C1986	L5	TSdU	salar	0.191	0.005	⁴⁰ Ar/ ³⁹ Ar	biotite	Université de Nice — Sophia-Antipolis	Bern 4B biotite, N/A	fusion + isochron	20	reference	known
Salar de Uyuni - C1999	TSdU	L5	salar	0.059	n/a	indirect U/Th of host sediment	halite	University of California?	N/A	AGE-MODE L	21	reference	known
SMS-15d	SMS-15d	-	channel	0.375	0.017	⁴⁰ Ar/ ³⁹ Ar	biotite	Sernageomin	FC; Steiger & Jäger (1977)	plateau	22	SERNAG EOMIN	known
T3	SGL3	-	alluvial fan	0.080	n/a	indirect - sediment OSL dating	N/A	University of Cologne	N/A	AGE-MODE L	23	CRC	new
TA-7-8	TA-8	-	channel	0.240.310	0.066	⁴⁰ Ar/ ³⁹ Ar	biotite	GEOMAR Kiel	TCR-2	plateau	3	reference	known
TA-7-8	TA-7	-	channel	0.098	0.042	⁴⁰ Ar/ ³⁹ Ar	biotite	GEOMAR Kiel	TCR-2	plateau	3	reference	known
TJ09-PdT1	TJ09-PdT1	-	playa	not dated	not dated	N/A	N/A	N/A	N/A	N/A	-	T. Jordan	new
TOC14/001	TOC14/001	-	alluvial fan	not dated	not dated	N/A	N/A	N/A	N/A	N/A	-	CRC	new

3.2 Samples and chronological and geochemical data

TephAta ~~sets a focus~~focuses on tephra samples from the Atacama Desert and adjacent regions, namely the Coastal Cordillera, the Central Depression, Precordillera and parts of the Western Cordillera ~~independent regardless~~ of their age. ~~Until now~~To date, the dataset primarily includes mainly tephra samples ~~were included, which are assigned to from~~ the late Middle Pleistocene to Late Pleistocene, ~~largely collected and were collected mainly~~ during field campaigns within the CRC1211 (2013-2023). ~~These S~~samples are derived from sites, which were within the scientific focus areas of CRC1211 subprojects and ~~from~~ adjacent sites to create a broad data foundation for characterizing major eruptive events and developing a ~~tephrostratigraphic tephrochronological framework and to characterize major eruptive events. This framework. This~~ set of samples was augmented by identifying tephra sites on geological maps and/or described in literature. ~~Where~~In case that tephra layers were identified ~~in the vicinity near of an~~ investigated CRC1211 archives or ~~shared of~~ similar ages, sample splits were requested from the Chilean National Geology and Mining Survey (SERNAGEOMIN) or the respective researchers of literature sources. If material could not be provided, respective sample sites were ~~tried to be~~ revisited and resampled during field ~~campaigns of the~~ CRC1211 field campaigns. TephAta also allows the integration of legacy data ~~reported in the literature for samples which are physically not available anymore for samples that are not accessible. Given their diverse origins across~~ different projects and decades, the currently investigated samples lack a standardized initial collection protocol. ~~The samples, which are currently investigated, have a heterogeneous origin from different projects and decades and related metadata and field observations were originally not collected based on a standardized protocol. Consequently, TephAta has been designed to accommodate this heterogeneity within a unified framework by offering a comprehensive set of optional data fields that can be utilized as information becomes available. Metadata and morphological field descriptions were extracted from references, field notes, or provided by personal communication. TephAta has been designed to accommodate the diverse range of data types within a single, unified framework. This is achieved by offering a comprehensive set of optional data fields, which can be utilized if needed and data is available. Metadata and morphological field descriptions of sites and samples were extracted from references and field notes or provided by personal communication.~~

285 Chronological data

Available ages for the samples currently included in ~~TephATA~~ TephAta have been extracted from published data and were complemented by new chronological results. Available ages from literature were obtained by $^{40}\text{Ar}/^{39}\text{Ar}$, K-Ar and U-Pb dating, but also inferring indirect tephra ages by dating the host sediment. Available details of the respective dating techniques, age calculations and references are stored sample-specific within TephAta and are summarized in Table 1.

290 For two samples (PAG-T4 and IRU-1a) new ages were obtained by $^{40}\text{Ar}/^{39}\text{Ar}$ multi-grain fusion dating of biotite at the Vrije Universiteit Amsterdam and are presented here for the first time. Mineral separates were achieved by sieving, magnetic separation, and hand picking before the selected mineral separate was packed in a 6 mm ID Al packages and loaded in a 25 mm ID Al cup together with Fish Canyon Tuff sanidine (FCs) standard. Sample and standard were irradiated at the Oregon State University TRIGA reactor in the cadmium shielded CLICIT facility for 7 hours (irradiation code VU114 and 15-OSU-295 06). At Vrije Universiteit Amsterdam after irradiation, samples and standards were unpacked and loaded in a 185 hole Cu tray and baked overnight at 250 °C under vacuum. This tray was then placed in a doubly pumped vacuum chamber with Zn-Se window and baked overnight at 120 °C under high vacuum. This chamber is connected to a ThermoFisher NGPrep gas purification line equipped with a hot GP50, a cold finger (Lauda at -70 °C) and hot St707 getter. Samples (1-3 grains/fusion) and standards (1 grain/fusion) are fused using a 25 W Synrad CO₂ laser. Released gas is analyzed on an ARGUS VI+ noble gas mass spectrometer, equipped with four Faraday cups at the H2, H1, AX and L1 positions and two compact discrete dynodes (CDDs) at positions L2 and L3. The system is equipped with a 1012 Ohm amplifier on H2 and 1013 Ohm amplifiers on H1, AX and L1 cups. Samples were run on H1-L3 collectors. Similar to Phillips and Matchan (2013), no bias corrections were applied, but samples and standards were analyzed in the same tray (and thus at more or less the same time) alternating with air

305 pipettes with intensities in the same range as the samples and standards. Line blanks were measured every 2-3 unknowns and were subtracted from succeeding sample data. Data reduction is done in ArArCalc (Koppers, 2002). Ages are calculated with decay constants of Min et al. (2000) and 28.201 Ma for FCs (Kuiper et al., 2008). The atmospheric $^{40}\text{Ar}/^{36}\text{Ar}$ air value of 298.56 is used (Lee et al., 2006). The correction factors for neutron interference reactions are $(2.64 \pm 0.02) \times 10^{-4}$ for ($^{36}\text{Ar}/^{37}\text{Ar}$) Ca, $(6.73 \pm 0.04) \times 10^{-4}$ for ($^{39}\text{Ar}/^{37}\text{Ar}$) Ca, $(1.21 \pm 0.003) \times 10^{-2}$ for ($^{38}\text{Ar}/^{39}\text{Ar}$) K and $(8.6 \pm 0.7) \times 10^{-4}$ for ($^{40}\text{Ar}/^{39}\text{Ar}$) K. All errors are quoted at the 2σ level.

310 Geochemical data

Depending on individual sample properties, different preparation methods were applied to enrich volcanic glass fragments for geochemical analyses. These methods include classical preparation techniques, like crushing of lithified/solidified samples, rinsing, (wet-) sieving, magnetic and density separation, and hand picking. Specific information for each sample is listed in the sample description and is also given along with the analytical results within the data-files provided for download (e.g., 315 results of geochemical ~~EPMA-WDS~~ analyses). Respective aliquot fractions enriched in glass fragments were mounted on epoxy pucks and polished to remove potential surficial alteration and to avoid topographic effects causing compositional variations during subsequent glass geochemical analyses.

~~The pucks were carbon coated for major and minor element analyses of glass by For~~ electron microprobe wavelength dispersive spectroscopy (EPMA-WDS) and/or scanning electron microscope energy dispersive spectroscopy (SEM-EDS) ~~the pucks were carbon coated and analyzed for their major and minor element glass composition. Specific methodological details for each sample are provided alongside the geochemical datasets in TephAta.~~

320 A JEOL JXA-8900RL electron microprobe equipped with five-wavelength dispersive spectrometers was used for these analyses at the University of Cologne (UoC). The operation conditions were set to 12 kV accelerating voltage, 6 nA beam current and 5 μm beam diameter. Full details of calibration and measuring conditions are given in Leicher (2021). Data reduction included ZAF correction and substitution of halogens (Cl, F) for oxygen using the JEOL Ltd JXA8900 Basic Software V3.02. Only EPMA-WDS geochemical analyses of glass fragments with analytical totals >90 wt.% were considered and normalized to 100% on a loss on ignition free basis, excluding volatiles (Cl, SO₂ and F).

~~Samples indicating the presence of multiple geochemical populations or trends of magmatic evolution within the EPMA-WDS glass composition data were further analyzed by SEM-EDS, if subject to LA-ICP-MS trace element analyses.~~

330 ~~For these samples, the same glass fragments analyzed by LA-ICP-MS were investigated for their major and minor element composition. The focus was to obtain grain specific SiO₂ concentrations, which were then used as internal standard during LA-ICP-MS trace element data reduction.~~

At the UoC, a Zeiss Sigma 300-VP equipped with an OXFORD Instruments EDX detector controlled by the software Aztec 4.1 was used for SEM-EDS analyses. The instrument was set to 20 keV and an image resolution of 512*512 pixel was chosen. 335 The number of channels was set to 2048, processing time to 5, with a dwell time of 10000 μs . The size of the scanning frame ~~or line~~ was adjusted to the respective grain size and typically exceeded 10 μm .

Trace-element analyses of glass fragments were performed at the University of Bonn (UoB) and UoC on the same sample pucks as the EPMA-WDS/SEM-EDS analyses, after removing the carbon coating. At the UoB trace element analyses were performed using a Resonetics Resolution M50E 193 nm excimer laser ablation system coupled to a Thermo Scientific Element 340 XR (Leicher and Lagos, 2021). A spot size of 26 μm was chosen and analyses were performed at a repetition rate of 5 Hz and a count time of 35 sec on the sample after 30 sec on the gas blank (background). A He gas flow (0.75 l min^{-1}), mixed together with Ar sample gas ($\sim 1.1 \text{ l min}^{-1}$) transported ablated material via an in-house signal-smoothing device to the ICP-MS. Maximum intensity as well as stability of the signal were obtained by tuning while taking account of concurrently low oxide ratios (ThO/Th of ~ 0.0012) to minimize potentially interfering oxide species prior to analyses in low-resolution mode. At UoC 345 an NWRimageGEO 193 nm ArF excimer laser ablation system coupled to a Thermo Scientific iCAP quadrupole or iCAP triple quadrupole ICP-MS was used for trace-element analyses. Individual glass fragments were analyzed using 15 or 20 μm

spot size, a repetition rate of 6 Hz and a count time of 40 sec on the sample after 30 sec of the gas blank (background) measurements. The sample aerosol was taken up by a He gas flow (0.9 l min⁻¹) and mixed with Ar (0.8 l min⁻¹), within a glass smoothing device before introduction into the plasma.

350 All data reduction was performed using the software Iolite 4.3 (Paton et al., 2011). The standard glass NIST SRM 612 was used for calibration and calculation of trace element concentrations based on ⁴³Ca, ⁸⁵Rb, ⁸⁸Sr, ⁸⁹Y, ⁹⁰Zr, ⁹³Nb, ¹³⁸Ba, ¹³⁹La, ¹⁴⁰Ce, ¹⁴¹Pr, ¹⁴⁶Nd, ¹⁴⁷Sm, ¹⁵³Eu, ¹⁵⁷Gd, ¹⁵⁹Tb, ¹⁶³Dy, ¹⁶⁵Ho, ¹⁶⁶Er, ¹⁶⁹Tm, ¹⁷²Yb, ¹⁷⁵Lu, ¹⁷⁸Hf, ¹⁸¹Ta, ²⁰⁸Pb, ²³²Th, ²³⁸U, ~~and incorporating As an internal standard ²⁹Si was incorporated as an internal standard using median SiO₂ concentrations obtained from EPMA-WDS data of respective samples. Since major and minor elements such as Ti, Na, K, or P were not analyzed by~~

355 ~~LA-ICP-MS, they could not be considered for detection of potential contamination by mineral phases during ablation. However, during data reduction in Iolite, the full analyzed trace element spectrum and Ca were screened to identify and exclude potential mineral inclusions (e.g. relatively elevated Ca, Sr, or Ba counts indicating feldspar inclusions) from data selection.~~

~~Si concentrations were obtained by EPMA WDS or SEM EDS and either considered as median values for samples with a narrow and homogenous silica composition or as grain specific values for tephra samples with heterogeneous silica composition.~~

360

The here presented geochemical data can be either downloaded as sample-specific datasets from the ~~TephATA~~ TephAta database (<https://www.crc1211db.uni-koeln.de/tephata>) or can be found as a combined dataset of all samples (~~Leicher N., 2026~~) deposited at EarthChem (Leicher N., 2026).

365 Data quality of geochemical analyses

During EPMA-WDS, SEM-EDS and LA-ICP-MS analysis MPI-DING standard glasses (ATHO-G, StHs6/80-G; Jochum et al., 2006) and SRM NIST SRM 610 (Jochum et al., 2011) were used as secondary standards to evaluate the accuracy and precision of individual measurement sessions. Sample-specific results of secondary standard analysis are stored within TephAta along with the sample results and are provided for download within the sample-specific data-file.

370 ~~Over the full analytical period, EPMA-WDS analyses conducted at UoC yielded mean intermediate precision (expressed as relative two standard deviation) and accuracy (expressed as bias relative to the preferred reference value)The overall timeframe of EPMA WDS analyses performed at UoC reveals mean values for intermediate precision (relative standard deviation %) and accuracy (bias of mean to preferred reference value in %) of up to 2.51.9 and 0.69 %, respectively, for elemental concentrations >75 wt.%, up to 4.42.1% and 0.61.1% for 75-12 wt.%, up to 13.337.4% and 1.22.0 % for 12-1 wt.% and up~~

375 ~~to 29.0-58.4 % and 5.96.4 % for <1 wt.%. Mean values for intermediate precision and accuracy of SEM-EDS analyses, respectively, are respectively both up to 0.36 and 0.3% for elemental concentrations > 75 wt.%, up to 13.9.8% and 0.3 % for 75-12 wt.%, up to 918.0 % and 3.7 % for 12-1 wt.% and up to 3060.0 % and 7.9 % for <1 wt. %. For the currently implemented legacy glass EPMA WDS data, evaluation of data quality is hampered by the lack of reported results of secondary reference materials (Placzek et al., 2009; Breitzkreuz et al., 2014). The respective legacy analyses stored in TephAta are flagged~~

380 ~~accordingly.~~

Secondary standard analyses of MPI-DING glasses ATHO-G and StHs6/80-G during LA-ICP-MS analyses at the UoB revealed median intermediate accuracies of <5 % for Sm, Ho, Rb, Ba, Pr, Ca, Sr, Ce, Yb, Lu, Hf, and Er, 5-12 % for La, Dy, Nd, Tm, U, Tb, Th, Eu, Y, Zr, Gd, Nb and Ta and 19 % for Pb. The median intermediate precision of the secondary standard analyses at UoB was typically ~~<5-10~~ % for Sr, Zr, Ce, Nb, Rb, Ba, La, Ca, Pr, Y, and Th and ~~510-14.28~~ % for Nd, U, Hf, Er,

385 Ho, Pb, Dy, Eu, Gd, Ta, Sm, Tb, Lu, Yb, and Tm. At the UoC, secondary standard analyses of MPI-DING glasses (ATHO-G, StHs6/80-G) glasses during LA-ICP-MS analyses revealed median accuracies of 5-10 % for Rb, Sr, Ba, Ca, Ce, La, Sm, Ho, and U, 10-15 % for Zr, Nd, Th, Hf, Y, Pr, Eu, Tb, Er, Yb, Nb, Dy Pb and 15-17 % for Gd, Lu, Tm and Ta. The median intermediate precision of the secondary standard analyses at UoC was typically < ~~5-10~~ % for Sr, Ba, Zr, Ce, La, Rb, Nb, Y, Ca, Pr, Nd, Th, Hf, Yb, U, Pb, Er, and Ta and of ~~510-8.16~~ % for Ho, Gd, Sm, Dy, Tb, Eu, Lu, and Tm.

390 4 Results and Discussion

4.1 Site and sample data

Currently, the ~~TephATA-TephAta~~ dataset lists 106 tephra samples from 91 tephra deposits sampled at 74 sites between approximately 20 – 27° S to 70-67°W. The specific origin (locality, reference) of samples is listed in Table 1. The set of samples includes 65 samples taken ~~previous to before~~ the CRC-research activities of which 23 samples originate from mapping
395 campaigns of the SERNAGEOMIN and 25 samples from other regional geoscientific studies. In addition, 17 previously known sample sites were revisited and re-sampled as part of the CRC's field work during ~~which also~~ which 41 newly identified tephra samples were gathered and included here.

Tephra samples are sourced from all types of sediment deposits of the Atacama Desert including alluvial fans, river terraces as well as clay pan and halite deposits. In addition, a small set of samples originating from the proximal deposits associated
400 with the Irruputuncu volcanic complex were included, because they represent a potential volcanic source. Sampling sites are mostly outcrops formed by the incision of channels, gravimetric movement, tectonic activity, and roadcuts, and also include pits and drill cores. Tephra deposits show a broad variety in their ~~morphology~~ physical properties, which represents the variable influence of eruption parameters and (post-) depositional related processes. The typical thickness of tephra layers is in the scale of centimeters, but also include several m-thick to sub-cm thin ~~(crypto-)~~ tephra deposits, whose lateral extent ranges from
405 decimeter to hectometer. In addition, cryptotephra horizons have been identified in sediment cores. -Visible volcanic ash layers are most commonly of bright color. Sedimentological texture properties, such as the grain-size, are in the range of ash for most tephra deposits, due to their distance to potential source volcanoes. Internal sedimentological structure of these tephra deposits, like grading, are only rarely observed due to their generally well-sorted grain-size distribution and are, if observed, commonly related to post-depositional weak water current transport processes. The mineralogical composition of tephra layers is
410 dominated by glass, but also primary (biotite, feldspar, zircon) and secondary minerals (gypsum, halite) were observed. The level of details of the available morphological description of individual layers varies, as for some samples morphological and mineral compositional details are incomplete.

4.2 Chronology of samples

Biotites of sample PAG-T4 were $^{40}\text{Ar}/^{39}\text{Ar}$ dated in two analytical sessions (19T04: n=10; 1-3 grains/hole; 19T11: n=20; 10
415 grains/hole) yielding individual weighted mean ages of 318.8 ± 18.9 ka (n=7 ages) and 298.4 ± 7.4 ka (n=18 ages), with a combined weighted mean age of 301.3 ± 13.8 ka. The weighted mean age is obtained by including as many individual analyses with mean squared weighted deviation (MSWD) < T-test statistic at 95 % confidence level. The $^{40}\text{Ar}/^{36}\text{Ar}$ inverse isochron intercept is 297.9 ± 1.0 and overlaps with air values of Lee et al. (2006). The analytical errors in the first series are larger due
420 to small beam intensities. The radiogenic ^{40}Ar yield is on average ~4 %. Biotites of sample IRU-1a were analyzed during the same analytical sessions (19T04: n=10; 1-3 grains/hole; 19T11: n=20; 4-5 grains/hole) as samples of PAG-T4 and their weighted mean age computation followed the same criteria. The first series yielded a weighted mean age of 188.7 ± 12.1 ka (n=6 ages) and the second series 171.2 ± 12.6 ka (n=7 ages), which gives a combined weighted mean of 180.5 ± 8.7 ka. The $^{40}\text{Ar}/^{36}\text{Ar}$ inverse isochron intercept is 298.1 ± 0.6 and overlaps with air values of Lee et al. (2006). The radiogenic ^{40}Ar yield
425 is very low with ~2 % on average. In the second series, parts of the experiments were discarded because the ^{40}Ar signal was too high for the detector and runs were aborted.

In combination with the data available in literature, 42 direct tephra ages obtained by absolute dating methods and 8 indirect tephra ages obtained by luminescence or U-Th dating of the host sediment, are available for 47 of 106 samples (Table 1, 3
430 samples have multiple ages). Of the 42 direct ages, the majority derives from biotite $^{40}\text{Ar}/^{39}\text{Ar}$ dating (n=29), whereas the other ages were obtained by biotite K-Ar (n=10), feldspar K-Ar (n=1), feldspar $^{40}\text{Ar}/^{39}\text{Ar}$ (n=1) and zircon U-Pb (n=1) dating methods.

The samples so far included in TephAta cover an age range from 22.90 to 0.06 Ma. Most samples (n=45) have an age < 1 Ma, but few samples (n=5) have Early Pleistocene to Miocene ages (Ritter et al., 2018; Medialdea et al., 2020). The ages of tephra layers >1 Ma suggest several distinct eruptive events, whereof only the ages of two samples partly overlap due to their 435 uncertainties of up to 21 % (CH22-NL-T1 and -T2, cf. Table 1). The $^{40}\text{Ar}/^{39}\text{Ar}$ sanidine of tephra layer SALAR T6 age

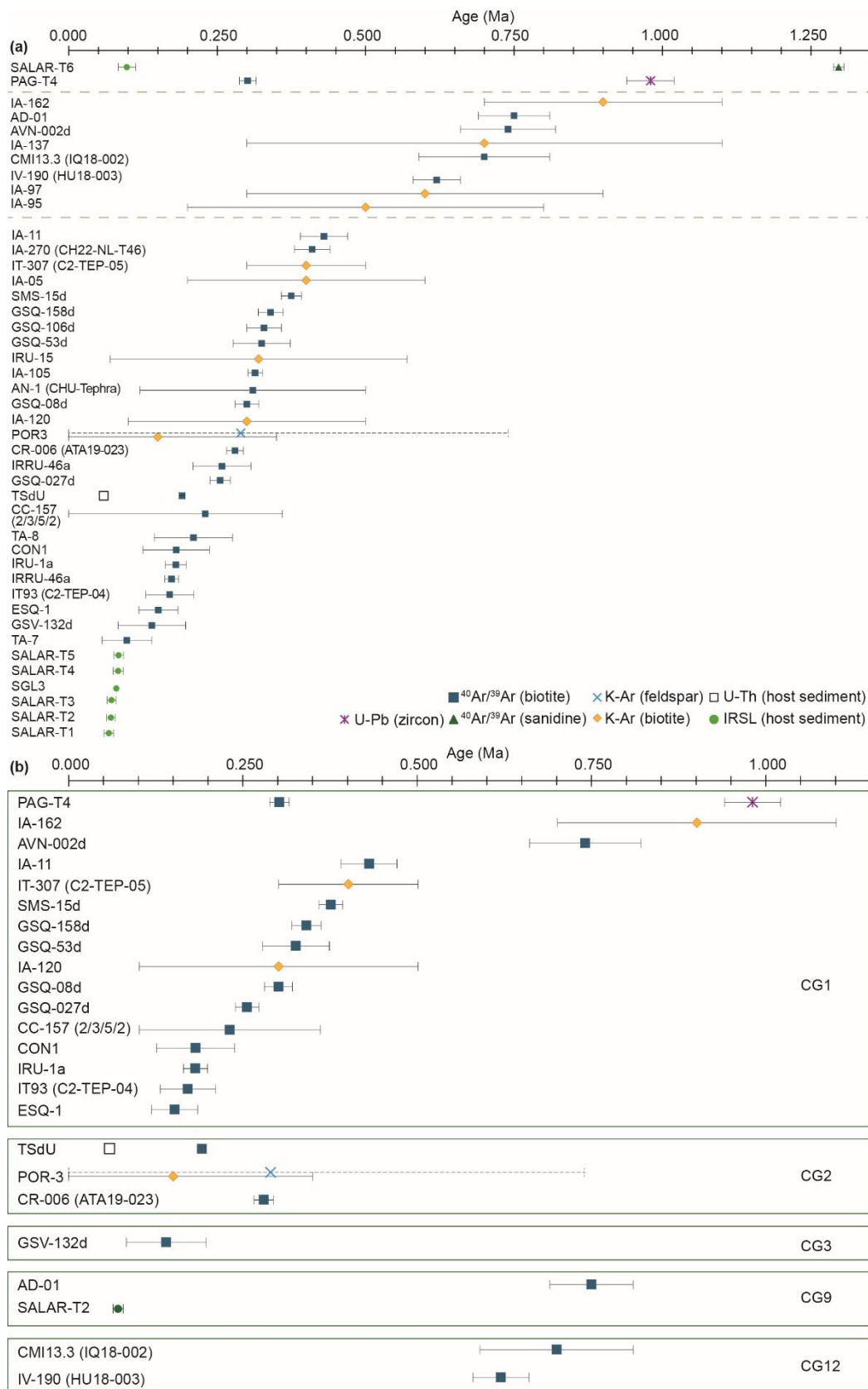


Figure 2: (a) Compilation of available chronological information for the samples of the Pleistocene being currently available within TephATA. For the references of the respective ages see Table 1. (b) Result of combined chronological and geochemical information illustrating the ages available for compositional groups CG 1, 2, 3, 9, and 12. The legend illustrates the different dating techniques used for the respective samples in a and b.

(1.297±0.018 Ma) is contradicted by a much younger IRSL host sediment age (<0.1 Ma), which is discussed in detail below. Among the <1 Ma old tephra layers, two main periods of explosive volcanic activity can be tentatively identified within the dataset (Fig. 2a). The older period includes tephra with ages of 0.9-0.5 Ma (n=7) and clustering between 0.75 and 0.60 Ma. The younger period includes samples with continuously overlapping ages between 0.43 and 0.06 Ma (n=36). One tephra deposit (PAG-T4) could not be assigned to one of these two periods, as different dating techniques provide very different ages with the new ⁴⁰Ar/³⁹Ar biotite age of 0.301±0.007 Ma and an U-Pb zircon age of 0.98 ± 0.04 Ma (Ritter et al., 2018). In general the active periods were also identified based on a partly overlapping dataset of chronological data focusing on tephra layers of the Coastal Cordillera of 20-21° S (Sepúlveda et al., 2013; Quezada et al., 2018).

Using solely the chronological data within the ~~TephATA-TephAta~~ dataset to disentangle and identify individual volcanic events <1 Ma within the two periods of volcanic activity is challenging. The heterogeneous dating techniques applied within several decades (1978-2023) used a variety of instruments, protocols, internal standards, and respective reference values, which limit the accurate differentiation of similar ages. A homogenization, e.g., through recalculation of ages based on the same reference values for mineral standards and decay constants, to increase the comparability of the complete dataset is, however, hampered by scarcity of metadata and is further limited by the fact that different dating methods have been applied. Besides the uncertainties related to the different methodological approaches, also the sample-specific aspects (quantity and quality of minerals, type of target minerals, plateau vs isochrone ages) infer further ambiguity in comparing their ages. 20 samples have relatively large age uncertainties of more than >15 %, which is especially evident within the group of K-Ar ages. Furthermore, due to uncertainties exceeding the respective dated ages, some (n=2) ages have to be classified as unreliable.

The ages of 7 samples assigned to the older period (0.5-0.9 Ma) overlap among each other within their uncertainties and do not allow a further differentiation. Among the younger sample group (<0.5 Ma), relatively small uncertainties of a few ages (SMS-15d: 0.375±0.017 kaMa, GSQ-08d: 0.300±0.020 kaMa, GSQ-027d: 0.255±0.017 kaMa, TdSU: 0.191±0.005 kaMa and IRU-1a: 0.1810.5±0.0098.7 kaMa) indicate a potential chronological differentiation into multiple eruptive events. All other ages of tephra layers, however, widely overlap with the aforementioned more precise ages and among each other, which hampers the assignment of tephra to a specific eruptive event. The age differences between some samples are within a range of 1-2 ka (e.g., GSQ-158d: 0.361-0.319 kaMa vs GSQ-08d: 0.320-0.280 kaMa; Fig. 2a), which is too small for a clear differentiation between eruptive events. Moreover, also the accuracy of the (more precise) ages is difficult to assess as their ages are based on a single, multi-grain incremental heating experiment, from which a plateau age was calculated. This limits the detection of sources for potential biases such as xenocryst contamination, incorporation of altered minerals or minerals with a complex crystallization history (Hora et al., 2010; Kern et al., 2016). Such biases are suggested for some samples, whose ⁴⁰Ar/³⁶Ar values are above the uncertainties of the atmospheric air value and thus indicate excess Ar, so that only inverse isochrone ages could be computed (e.g., IA-11, SMS-15d). Considering the few available total fusion ages within the dataset (PAG-T4, IRU-1a), their individual ages show a natural scatter in ages and thus provide additional information to extrapolate more robust eruption ages, while potential biased ages (e.g. several age populations caused by xenocrysts) can be filtered. Among the here listed samples, only very few samples have been dated by different dating approaches to further test for potential biases. The available results indicate inconsistencies such as by the zircon U-Pb age for tephra PAG-T4 of 0.98±0.04 Ma (Ritter et al., 2018), which is in conflict with the ⁴⁰Ar/³⁹Ar biotite age of 0.301±0.06 Ma obtained from the same sample. The youngest tephra ages included in the dataset derive from a series of indirect infrared stimulated luminescence (IRSL) ages of the respective outcrop. The stratigraphic oldest tephra layer of this deposit (SALAR T6) has been also dated by sanidine ⁴⁰Ar/³⁹Ar (Medialdea et al., 2020) yielding a weighted mean age of 1.297±0.018 Ma is based on a robust population of 25 individual total fusion ages. However, this age is much older than the proposed IRSL maximum age <0.098±0.015 Ma and was explained by the authors as a potential reworking of the tephra layer (Medialdea et al., 2020). New tephrostratigraphic conclusions based on new geochemical signatures (discussed below), however, question this hypothesis. Further, the geochemical fingerprint of an overlying tephra (SALAR-T2) in the succession likely corresponds to a tephra dated at 0.75±0.06

Ma, thus also indicating an older age of the sequence. A similar situation is observed for a tephra found in drill cores from Salar de Uyuni, where the directly obtained biotite $^{40}\text{Ar}/^{39}\text{Ar}$ age of the tephra is in conflict with a younger age derived from the U-series and ^{14}C -based age model of the succession (Fornari et al., 2001; Fritz et al., 2004). Overall, the uncertainties and inconsistencies between the different dating approaches make a chronological differentiation between all available ages only of a tentative nature and suggest the need for additional criteria (e.g., other dating methods, geochemical fingerprinting) for a robust separation into different eruptive events.

485

4.3 Geochemistry

For 79 of the 91 sites being listed within TephAta, glass geochemical compositions of tephra layers are available, which were obtained from ~~83-82~~ of the 106 samples. 65 of these samples were geochemically characterized for the first time and ~~16-15~~ samples had been characterized within the scope of previous projects within the CRC (May et al., 2020; Medialdea et al., 2020; Ritter et al., 2022). In addition, for two samples EPMA-WDS legacy data (2/3/5/2, AD-01; Placzek et al., 2009; Breitreuz et al., 2014) and new measurements are available. ~~For samples listed with an incomplete or missing geochemical characterization, the pending major, minor, and/or trace element analyses data will be complemented within the successive analytical work of the CRC1211.~~ Comparing the legacy data with the respective new EPMA-WDS analyses reveals that the major and minor glass compositions of AD-01 are undistinguishably overlapping. However, the legacy data of sample 2/3/5/2 has significantly higher SiO_2 values (79.25-81.22 wt.%) compared with its reanalysis data (74.40-77.93 wt.% SiO_2), which results also in differences observed for the other element concentrations. A significant alkali loss and a SiO_2 -enrichment were already noted in Breitreuz et al. (2014), but the reason for such could not be explained. With regard to the high SiO_2 concentrations of the 2/3/5/2 legacy data, similarly high values were not observed for other samples within TephAta. Since no secondary reference data are given in the original article, a technical issue cannot be excluded.

500 Major and minor element compositions of the samples allow a general classification of their composition based on the Total Alkali vs. Silica diagram (TAS, Le Bas et al., 1986) ~~suggesting that: Except for sample SALAR T3 (basaltic trachyandesite),~~ all samples are dominated by glass shards ~~having with~~ rhyolitic compositions (Fig. 3). ~~Seven-Five~~ of these samples (SGL3, IRRU13, ~~TSdU, SALAR T5,~~ PAG17 ID4, ID14, ID24) have a more heterogeneous composition including also less evolved trachyandesitic, trachytic and/or dacitic shards. The samples of rhyolitic compositions exhibit silica concentrations which suggests a subdivision into three silica-types: type I (n=66) includes samples dominated by shards with silica concentrations between ~76-79 SiO_2 wt.%, type II (n=7) between ~73-76 SiO_2 wt.% and type III (n=9) represents a mix of both types having less homogenous rhyolitic compositions. This classification is also seen within the other major and minor element data of the samples investigated, as samples of the same silica type have very similar, partly overlapping major and minor oxide compositions (Fig. 3).

510 The majority of the rhyolitic type I samples have a similar major and minor element geochemical composition and cannot be further separated into different geochemical clusters. Some samples of type I, however, show specific variations in TiO_2 , $\text{FeO}_{(\text{TOT})}$, CaO , K_2O and/or Na_2O concentrations, which suggest a division into several clusters (Fig. 3b, d, g-i). Tephra samples of type II and type III cannot be further separated into compositional clusters based on their major element glass geochemistry, except for individual differences observed within the CaO content (Fig. 3d,e; e.g., SALAR T4~~2~~, SG17/002, TJ09-PdT CH18-
515 T3, CH18-T5).

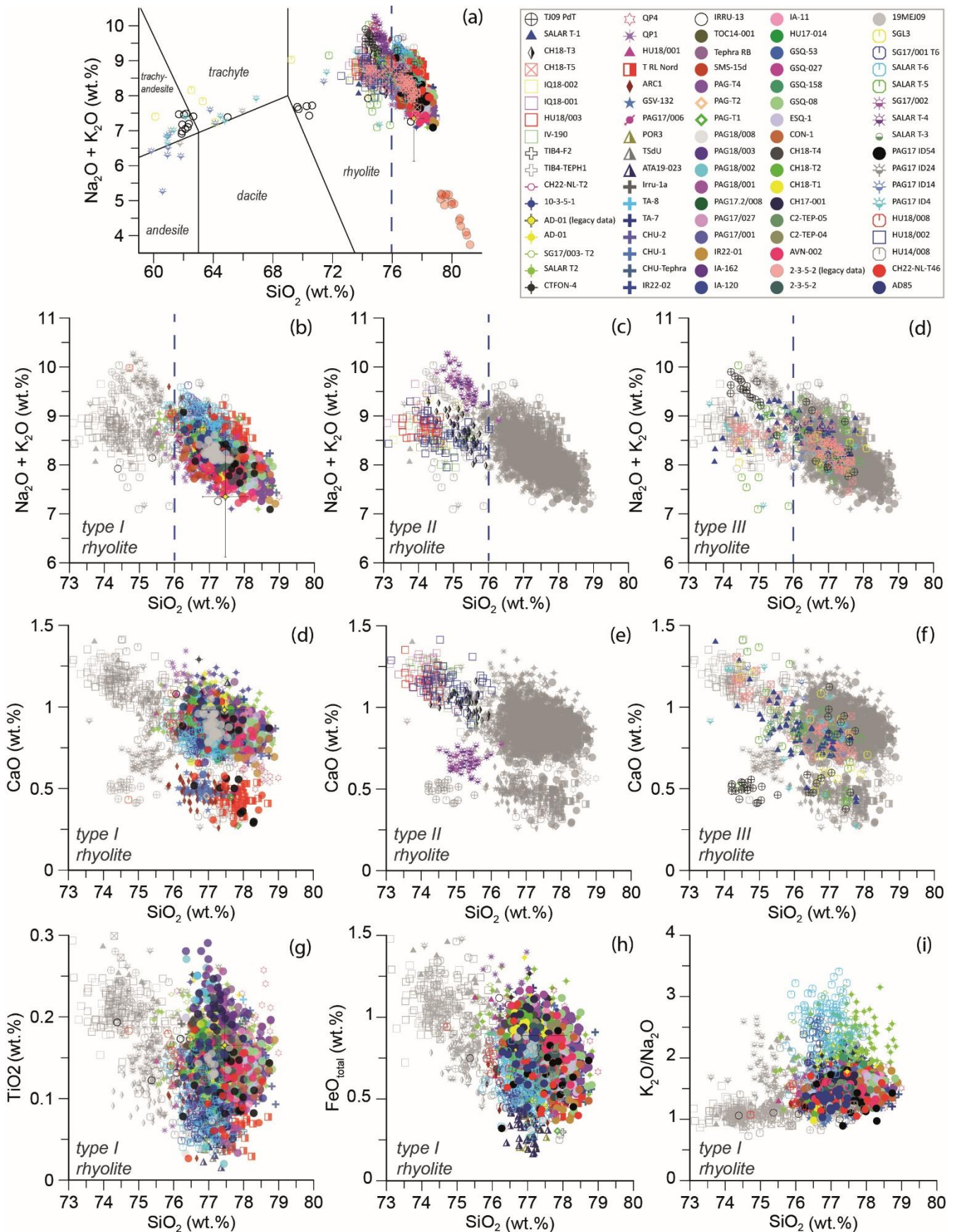


Figure 3: Geochemical classification and differentiation based on major and minor element glass compositions of the investigated tephra layers. (a) TAS-classification of all samples according to Le Bas et al. (1986). (b-c) TAS-diagram extraction for differentiation between type I, II and III rhyolites according to their silica content. (d, g-i) x-y oxide plots indicating a differentiation of type I rhyolites according to differences in the CaO, TiO₂, FeO_{total} compositions (wt.%) and Na₂O/K₂O alkali-ratio. (d,e) x-y oxide plots indicating internal differentiation of type II and III rhyolites according to differences in the CaO (wt.%) composition of respective samples.

~~A more detailed geochemical fingerprint of an eruptive event can be provided by their trace element glass shard composition~~
520 ~~(!!! INVALID CITATION !!! (Tomlinson et al., 2012b; Pearce, 2014; Hopkins et al., 2021)).~~ Due to their generally more
~~incompatible behaviour and lower concentrations of trace elements compared to major and minor elements within the melt,~~
~~trace elements effectively amplify compositional variations driven by differences in the parental magma source and magmatic~~
~~history (e.g. fractional crystallization, degree and depth of melting, or residual mineral assemblages).~~ Thus, trace element
525 ~~geochemistry of glass shards have been shown to be a reliable parameter for distinguishing between eruptions with similar~~
~~major element composition (Tomlinson et al., 2012b; Pearce, 2014; Hopkins et al., 2021).~~ ~~A more detailed geochemical~~
~~fingerprint of an eruptive event can be provided by their trace element glass shard composition~~
~~Due to the more incompatible behavior of trace elements compared with major elements during magmatic differentiation (e.g.~~
~~enrichment/depletion by partitioning into mineral phases or melt during crystal fractionation/partial melting), these~~
~~concentrations can provide a more diagnostic feature to distinguish between geochemical similar eruptions.~~ For better
530 differentiation among the identified geochemical clusters and to identify potential additional compositional differences, trace
element data of ~~64-59~~ samples were considered. The individual samples show a mostly homogenous composition or indicate
geochemical trends supporting that samples represent primary deposits and no mixture of different eruptions. Trace-element
concentrations normalized to values of the primitive mantle (pyrolite; McDonough and Sun, 1995) reveal for all samples (Fig.
4a-c) a relative enrichment of large-ion lithophile elements (LILE: Rb, Ba, Pb) against high field strength elements (HFSE:
535 Ta, Nb, Hf, Zr), and among the latter an enrichment of light REE (LREE) compared to heavy REE (HREE), which is a pattern
typical for the geodynamic continental arc setting. Combining the major, minor and trace element data enables the definition
of 16 clusters, which are shortly discussed below and are listed in Table 2.

Among the ~~57-52~~ individual trace-element data sets of type I rhyolites, a differentiation into 11 different clusters is suggested
due to distinct differences in their trace-element compositions (Fig. 4). Among them, ~~40-35~~ samples have a ~~homogenous~~
540 overlapping composition and are grouped in compositional group (CG) 1, ~~which can be further subdivided (Fig. 4d,e) into a~~
~~narrow homogenous population of 33 samples (CG1.1) and a group of seven samples generally having a similar composition,~~
~~but with a wider range (CG1.2).~~ CG-2 comprises four samples of which three are compositionally identical (CG2.1), whereas
one sample shows a generally similar pattern, although with differences in composition (CG2.2). All samples can be clearly
distinguished from the other CGs by their lower HFSE and REE concentrations (Fig. 4a-c). Compositional groups 3, 4, 5, 6,
545 7, and 8 include one sample each, which all differ among each other (Fig. 4a-c, f-i). CG3 tephra has low Th concentrations (5-
10 ppm) and a certain enrichment in HFSE (Y, Nb) and HREE compared with the other type I rhyolites, which is also observed
for CG4. A characteristic depletion in Sr and Ba accompanied by elevated HFSE (except for Zr, Hf) and HREE separate CG5
from the other clusters. CG6 has slightly enriched Ba concentrations as well as HFSE and LREE, if compared to CG1. CG7
and CG8 both have a wider range of composition and have slightly lower LILE, but higher HFSE and (H+L)REE
550 concentrations. CG9 includes four different tephra samples with a common composition, having generally higher Th
concentrations (25-40 ppm, compared to 15-26 ppm of CG1.1), and further differ e.g. from CG1 by higher HFSE (Y, Nb, U)
and LREE (La, Ce, Pr, Nd). CG10 has, relative to other rhyolite I tephra, lower Sr and Ba, but elevated HFSE (Y, Nb, Ta, U)
and HREE concentrations, similar to tephra composition of CG11.

The individual trace element compositions of type II rhyolites (n=3) overlap, such as their major-element compositions, and
555 thus are grouped as CG12. Their trace element compositions clearly differ from those of the other rhyolites (type I+III) as seen
e.g., in lower LILE (except for Ba, Sr) and higher HREE. Trace-element compositions of type III rhyolites (n=4) are
heterogeneous among each other and allow a differentiation into four individual clusters (CG13, 14, 15, 16). CG13 has low
HFSE and REE concentrations relative to other type III rhyolites. CG-14 and ~~CG~~15 are slightly similar and partially overlap
with CG12. However, they clearly differ in lower HFSE (Zr, Hf), higher U concentrations, lower HFSE (Zr, U), and higher
560 Ba concentrations.

Table 2: Overview of samples and their classification based on the Total Alkali vs. Silica composition (TAS; Le Bas et al., 1986), their assignment into rhyolites types I-III, and trace element compositional groups (TE-CG). If no trace element compositions were available, samples are listed at the end of each respective rhyolitic type. Samples which have not been geochemically investigated are listed at the bottom of the table.

TAS Group	CG-TE	samples					
basaltic-trachyandesite	not analyzed	Salar-T3	-	-	-	-	
rhyolite "type I"	1.1	19MEJ09	2/3/5/2	AVN-002d	C2-TEP-04	C2-TEP-05	
		CH17-001	CH18-T1	CH18-T2	CH18-T4	CON-1	
		ESQ-1	GSQ-027d	GSQ-08d	GSQ-158d	GSQ-53d	
		HU17-014	IA-11	IA-120	IA-162	IR22-001	
		IR22-002	PAG17.2-008	IRU-1a	PAG17.2-008	PAG17/001	PAG17/027
		PAG18/001	PAG18/002	PAG18/003	PAG18/008	PAG18/008	PAG-T1
		PAG-T2	SMS-15d	PAG-T4	SMS-15d	Tephra RB	TOC14/001
		CHU Tephra	TA-7	CHU-1	CHU-2	IR22-002	IRU-1a
		TA-7	TA-8				
		2.1	POR 3	TSdU	ATA19-023		
	2.2	PAG17/006					
	3	GSV-132					
	4	ARC1					
	5	Tephra RL N					
	6	HU18/001					
	7	QP1					
	8	QP4					
	9	10-3-5-1	AD-01	CTFON-4	SALAR T2		
	10	CH22-NL-T2					
	11	TIB4-Teph1	TIB4-F2				
not analyzed	AD-85	CH22-NL-T46	HU14-008	HU18-008	PAG17 ID54		
not analyzed	SALAR T6	SG17/001	SG17/003	IRRU-13	CHU Tephra		
	CHU-1	CHU-2	TA-7	TA-8			
rhyolite "type II"	12	IQ18-001	IQ18-002	IV-190			
	not analyzed	HU18/002	HU18/003	SALAR T4	SG17/002		
rhyolite "type III"	13	CH18-T5					
	15	SALAR T1					
	14	CH18-T3					
	16	TJ09-PdT1					
not analyzed	not analyzed	PAG17 ID4	PAG17 ID14	PAG17 ID24	SALAR T5		
not analyzed	not analyzed	19MEJ10	23MEJ1	AN1	CC157		
not analyzed	not analyzed	CH22-NL-T3-1	CH22-NL-T3-2	CMI13.3	CR-006A		
not analyzed	not analyzed	IA-05	IA-105	IA-137	IA-270		
not analyzed	not analyzed	IA-97	IRRU-46a	IRU-15	IS-155		
not analyzed	not analyzed	IT-93	IV-189	L5	CH22-NL-T1		
					GSQ-106d		
					IA-95		
					IT-307		

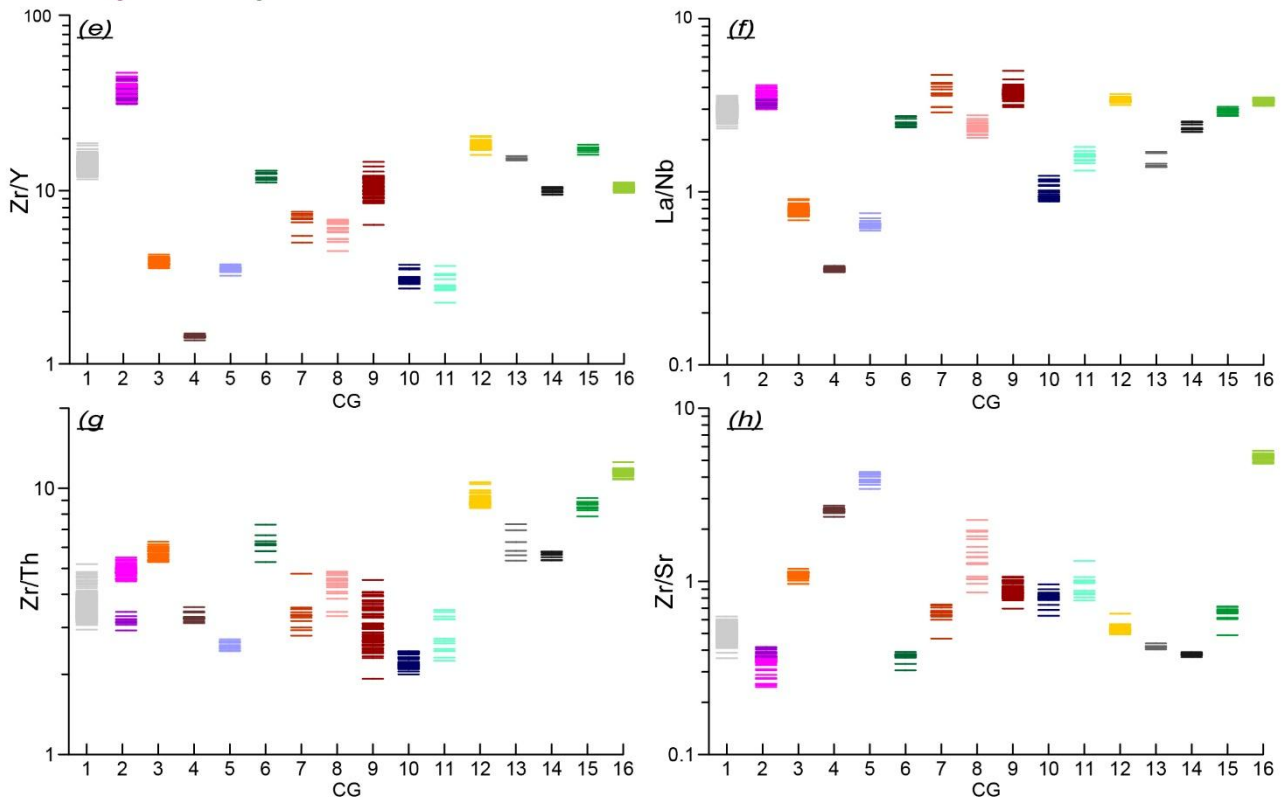
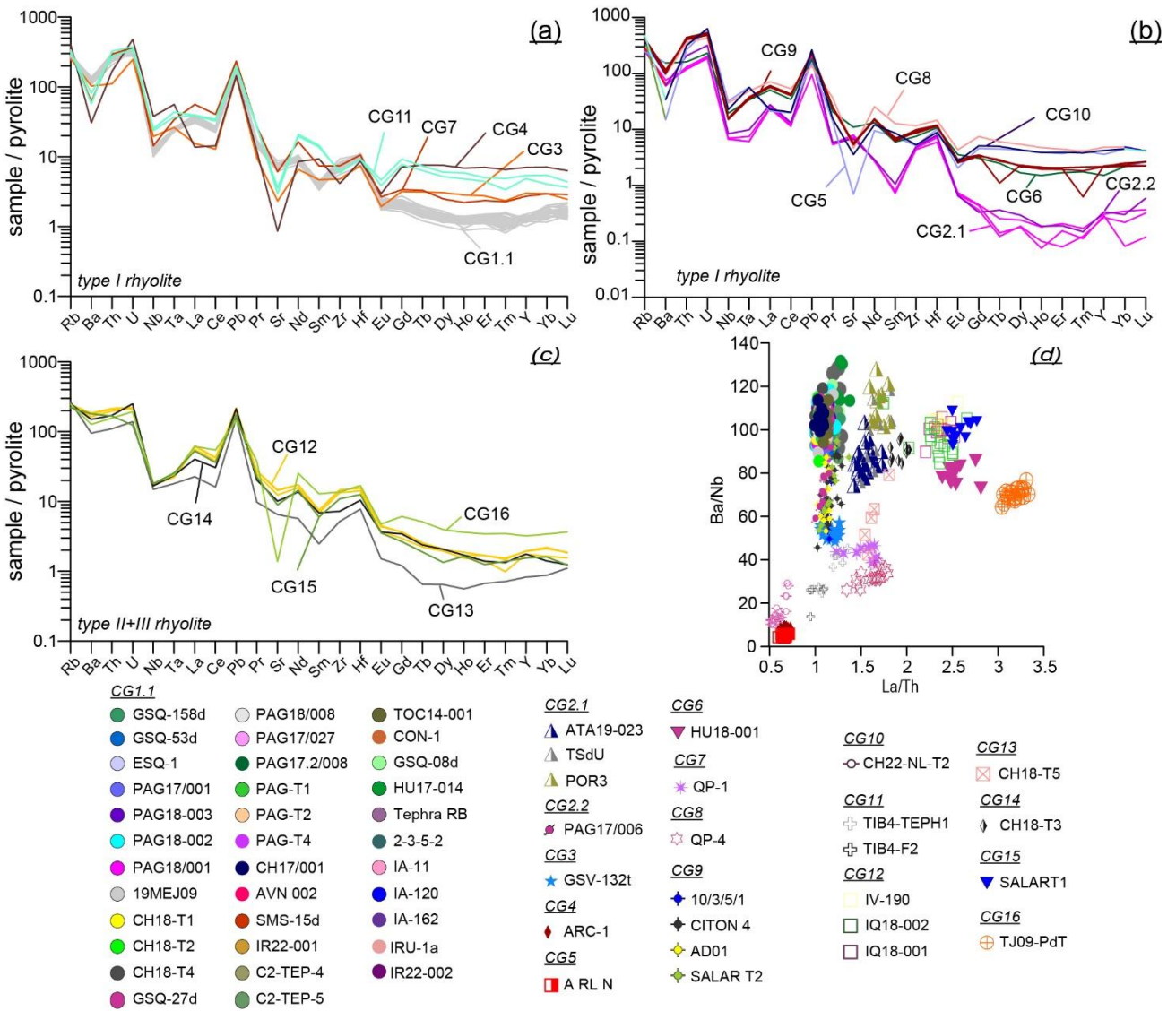


Figure 4: Geochemical classification and differentiation based on trace element glass compositions of investigated tephra layers. (a-c) Spidergrams demonstrating different degrees of enrichment/depletion of REE of the different composition groups. For each tephra sample the mean is given. Samples of the same composition group share the same color and are sorted according to their assignment to rhyolites I-III. Trace-element concentrations are normalized to values of the primitive mantle (pyrolite; McDonough and Sun, 1995). (d,e) x-y plots for trace element ratios La/Th vs. Ba/Nb to demonstrate the clustering of the different individual samples. (e) ~~Extract of x-y plot in (d) to demonstrate the differences between CG 1.1 and CG1.2 and to CG9.~~ (f-h) High-low plot of selected trace element ratios illustrating the differences between the different CG1-16. For each CG, all individual sample data are plotted as a stack.

~~Tephrostratigraphic and~~ chronological implications

570 The geochemical fingerprinting approach of tephra layers from the Atacama Desert enables the identification and characterization of distinct volcanic events, which promotes the investigation of inter-site tephra correlations and their spatial dispersal. A first assessment of the combined major, minor, and trace-element compositions of the tephra layers, allows a definition of 16 different geochemical clusters, which likely represent at least the same number of volcanic events. Some tephra layers were found in ~~widespread different sedimentary~~ archives (e.g., tephra layers of CG1, CG2, CG9). The widespread
575 dispersal of these tephra layers points to major eruptive events, which have the potential to become marker horizons within the sedimentary archives of the Atacama Desert. Even though for several tephra layers no ~~equivalents correlations with other~~ tephra deposits could be identified, their heterogenous geochemical clustering highlights their potential to contribute as geochemically distinct markers within the developing stratigraphic framework.

Although many of the investigated tephra layers have already been dated, the available chronological data often exhibit large
580 uncertainties, which hamper a clear differentiation between one or multiple volcanic events. This uncertainty can be refined by including the results of the geochemical clustering to verify or falsify the indicated age differentiation, but also to identify equivalent tephra layers of the same volcanic origin. For 7 of the 16 geochemically defined clusters chronological information is available and allows the assessment of ~~42-39~~ individual ages. Accordingly, at least 9 volcanic events have been identified for which no chronological information is available at present. As samples with ages >1 Ma have not been in the main focus
585 of this exemplary dataset, an in-depth tephrostratigraphic evaluation of these older events is not possible to date. Overall, the now available chronological and geochemical data are a valuable basis for further exploring the explosive volcanic history of the region between 22 and 1 Ma. First implications are that the geochemical fingerprinting of samples <1 Ma supports the identified bifurcation of active periods within the geochronological data and further allows to characterize individual events within the two activity periods (0.06-0.43 Ma and 0.5-0.9 Ma). For the samples >0.5 Ma, their assignment to different
590 geochemical clusters (CG9+12) indicates at least two different eruptive events. Although their age uncertainties overlap, the combined age limits of ~~equivalent correlated~~ samples suggest two eruptive events at ca. 0.75 Ma (CG9) and ca. 0.6 Ma (CG12). For the remaining samples, the clustering of their geochemical data implies three potential volcanic events.

Samples belonging to CG1 (n=~~4035~~) appear to be the most widespread cluster identified so far, but their available ages do not allow a distinct age constraint at present. Ages of CG1 include ~~17-14~~ ages with an age between 0.4-0.1 Ma, but also three ages
595 exceeding 0.5 Ma (Fig. 2b). Their geochemically indistinguishable compositions imply a single volcanic eruption, but some samples with more precise ages within this group tentatively suggest ~~a~~-multiple eruptions (PAG-T4, SMS-15d, GSQ-08d, GSQ-027d). Thus, it cannot be fully excluded that CG1 represents a group of repeating eruptions with identical geochemical composition that occurred in short succession. Regarding the other two identified eruptive events, no precise age can be given at present. For the older one (CG2), two differing ages of 0.191±0.005 Ma (L5/TdSU) and 0.280±0.014 Ma (ATA19-023/CR-
600 006A) exist, whereas for the younger (CG3) only an imprecise age of 0.140±0.057 Ma (GSV-132d) is available.

In some archives, ~~the tephrostratigraphic-tephrochronology approach via tephra correlation~~ also provides an independent validation of direct dating of host sediment. A tephra layer (SALAR T2) of the SALAR GRANDE hillslope section (Medialdea et al., 2020) now could be correlated with a tephra layer dated in other archives, introducing an additional age of 0.75±0.06
605 Ma for the succession. This age, however, is in conflict with the much younger IRSL ages from the section (<0.1 Ma), but rather supports the direct age obtained for the lowermost tephra of the succession (SALAR T6: 1.297±0.018 Ma; Medialdea

et al., 2020). The distinct geochemical compositions of all tephra layers in the succession associated with different geochemical clusters supports a primary deposition of those layers and rather contradicts a reworking of the dated sanidine crystals from older material (Medialdea et al., 2020). In a sediment core recovered from Salar de Uyuni, the biotite $^{40}\text{Ar}/^{39}\text{Ar}$ age of a tephra layer (0.191 ± 0.005 Ma; Fornari et al., 2001), is questioned by a much younger, indirect U-Th age of the host sediment (0.059 Ma; Fritz et al., 2004). This tephra layer could now be geochemically correlated with two other pyroclastic deposits being located westward of Salar de Uyuni (POR-3, ATA19-023) and of which the age of ATA19-023 (resampled CR-006A: 0.280 ± 0.014 Ma; Gardeweg and Sellés, 2013) is supporting also an older age. However, the large difference in their ages highlights the need for refining their chronology.

615

Data availability:

Table 3 (below) lists all samples included within this manuscript and provides their IGSN number and a link to download the individual geochemical data, which is stored within TephAtaTA (<https://www.crc1211db.uni-koeln.de/tephata>). In addition, the full dataset (meta and chronological data overview and geochemical data including individual major, minor and trace element glass compositions) is also made available for download at the EarthChem repository: <https://doi.org/10.60520/IEDA/114209>.

620

Sample	IGSN/DOI	SEM/EPMA data	LA-ICP-MS data
10-3-5-1	10273/GF1211S-94	YES	YES
19MEJ09	10273/GF1211S-4E	YES	YES
19MEJ10	10273/GF1211S-4F	not available	not available
2/3/5/2	10273/GF1211S-7	YES	YES
23MEJ1	10273/GF1211S-4H	not available	not available
AD-1	10273/GF1211S-97	YES	YES
AD-85	10273/GF1211S-7X	YES	not available
AN-1	10273/GF1211S-77	not available	not available
ARC1	10273/GF1211S-44	YES	YES
ATA19-023	10273/GF1211S-3H	YES	YES
AVN-002d	10273/GF1211S-33	YES	YES
C2-TEP-04	10273/GF1211S-Y	YES	YES
C2-TEP-05	10273/GF1211S-3-	YES	YES
CC-157	10273/GF1211S-79	not available	not available
CH17-001	10273/GF1211S-7-	YES	YES

CH18-T1	10273/GF1211S-9M	YES	YES
CH18-T2	10273/GF1211S-9N	YES	YES
CH18-T3	10273/GF1211S-9P	YES	YES
CH18-T4	10273/GF1211S-9R	YES	YES
CH18-T5	10273/GF1211S-9T	YES	YES
CH22-NL-T1	10273/GF1211S--C	not available	not available
CH22-NL-T2	10273/GF1211S--E	YES	YES
CH22-NL-T3-1	10273/GF1211S--F	not available	not available
CH22-NL-T3-2	10273/GF1211S--H	not available	not available
CH22-NL-T46	10273/GF1211S-3W	YES	not available
CHU Tephra	10273/GF1211S-34	YES	not available YES
CHU-1	10273/GF1211S-37	YES	not available YES
CHU-2	10273/GF1211S-39	YES	not available YES
CMI13.3	10273/GF1211S-7A	not available	not available
CON-1	10273/GF1211S--9	YES	YES
CR-006A	10273/GF1211S-7C	not available	not available
CTFON-4	10273/GF1211S-99	YES	YES
ESQ-1	10273/GF1211S--A	YES	YES
GSQ-027d	10273/GF1211S-3X	YES	YES
GSQ-08d	10273/GF1211S--J	YES	YES
GSQ-106d	10273/GF1211S-7E	not available	not available
GSQ-158d	10273/GF1211S--K	YES	YES
GSQ-53d	10273/GF1211S--L	YES	YES
GSV-132d	10273/GF1211S-3M	YES	YES
HU14/008	10273/GF1211S-7Y	YES	not available
HU17-014	10273/GF1211S-9A	YES	YES
HU18/001	10273/GF1211S-4U	YES	YES

HU18/002	10273/GF1211S-4V	YES	not available
HU18/003	10273/GF1211S-9-	YES	not available
HU18/008	10273/GF1211S-93	YES	not available
IA-05	10273/GF1211S-7F	not available	not available
IA-105	10273/GF1211S-7H	not available	not available
IA-11	10273/GF1211S--M	YES	YES
IA-120	10273/GF1211S--N	YES	YES
IA-137	10273/GF1211S-7J	not available	not available
IA-162	10273/GF1211S--P	YES	YES
IA-270	10273/GF1211S-7K	not available	not available
IA-95	10273/GF1211S-7L	not available	not available
IA-97	10273/GF1211S-7M	not available	not available
IQ18-001	10273/GF1211S-9E	YES	YES
IQ18-002	10273/GF1211S-9C	YES	YES
IR22-001	10273/GF1211S--T	YES	YES
IR22-002	10273/GF1211S-3A	YES	YES
IRRU-13	10273/GF1211S-4A	YES	not available
IRRU-46a	10273/GF1211S-7N	not available	not available
IRU-15	10273/GF1211S-7P	not available	not available
IRU-1a	10273/GF1211S-4C	YES	YES
IS-155	10273/GF1211S-7R	not available	not available
IT-307	10273/GF1211S-7U	not available	not available
IT-93	10273/GF1211S-7T	not available	not available
IV-189	10273/GF1211S-7V	not available	not available
IV-190	10273/GF1211S-7W	YES	YES
L5	10273/GF1211S-3K	not available	not available
PAG17 ID14	10273/GF1211S-4R	YES	not available

PAG17 ID24	10273/GF1211S-4T	YES	not available
PAG17 ID4	10273/GF1211S-4P	YES	not available
PAG17 ID54	10273/GF1211S--3	YES	not available
PAG17.2-008	10273/GF1211S-4J	YES	YES
PAG17/001	10273/GF1211S--U	YES	YES
PAG17/006	10273/GF1211S-9F	YES	YES
PAG17/027	10273/GF1211S-9H	YES	YES
PAG18/001	10273/GF1211S--V	YES	YES
PAG18/002	10273/GF1211S-47	YES	YES
PAG18/003	10273/GF1211S-49	YES	YES
PAG18/008	10273/GF1211S-9J	YES	YES
PAG-T1	10273/GF1211S-9K	YES	YES
PAG-T2	10273/GF1211S-9L	YES	YES
PAG-T4	10273/GF1211S--4	YES	YES
POR 3	10273/GF1211S-3J	YES	YES
QP1	10273/GF1211S-4-	YES	YES
QP4	10273/GF1211S-43	YES	YES
SALAR T1	10273/GF1211S-3N	YES	YES
SALAR T2	10273/GF1211S-3P	YES	YES
SALAR T3	10273/GF1211S-3R	not available	not available
SALAR T4	10273/GF1211S-3T	YES	not available
SALAR T5	10273/GF1211S-3U	YES	not available
SALAR T6	10273/GF1211S-3V	YES	not available
SG17/001	10273/GF1211S-4K	YES	not available
SG17/002	10273/GF1211S-4L	YES	not available
SG17/003	10273/GF1211S-4M	YES	not available
SGL3	10273/GF1211S-3F	YES	not available

SMS-15d	10273/GF1211S-- W	YES	YES
TA-7	10273/GF1211S- 3C	YES	not availableYES
TA-8	10273/GF1211S- 3E	YES	not availableYES
Tephra RB	10273/GF1211S-- X	YES	YES
Tephra RL N	10273/GF1211S- 3Y	YES	YES
TIB4-F2	10273/GF1211S- 4X	YES	YES
TIB4-TEPH1	10273/GF1211S- 4W	YES	YES
TJ09-PdT1	10273/GF1211S- 4N	YES	YES
TOC14/001	10273/GF1211S-- R	YES	YES
TSdU	10273/GF1211S- 3L	YES	YES

625 Conclusions

630 TephAta represents a new platform to support the development of a ~~thorough-comprehensive tephrostratigraphic tephrochronological~~ framework for the Atacama Desert in northern Chile. Its ~~comprehensive~~ structure is strongly aligned ~~to~~ ~~with intensively elaborated scientific tephra~~ guidelines ~~of the scientific tephra community~~ (Wallace et al., 2022) ~~and allows providing a centralized online repository for tephra related data. the storage of tephra-related information in a single~~ ~~online repository. As the first platform of its kind to integrate geochemical, geochronological, and detailed outcrop metadata, TephAta preserves both new and legacy datasets to maximize data reusability~~ ~~It is the first online repository, which incorporates geochemical and geochronological tephra data and makes detailed outcrop and sample descriptions available, including their metadata. Besides the documentation of new samples, TephAta is also meant to store legacy datasets, which will foster and simplify the reusability of existing datasets.~~ Due to the automatic implementation of IGSNs ~~for the samples~~, samples become

635 citable and have a unique identification, ~~facilitating interoperability with global repositories, which provides a link to incorporate datasets within other (global) databases to increase findability of data.~~ At present the dataset ~~includes-contains~~ information from 106 tephra samples. ~~For samples listed with an incomplete or missing geochemical characterization, the pending major, minor, and/or trace element analyses data will be complemented within the successive analytical work of the CRC1211. Future expansions will progressively incorporate over 400 additional samples from SERNAGEOMIN and current~~ ~~CRC activities. It is planned to progressively incorporate tephra data from SERNAGEOMIN and ongoing CRC activities, which already comprise more than 400 samples.~~ This set of samples will cover a time interval from the Early Miocene to the Holocene and has a spatial extent from the Chilean coast to the Andes along 18-30°S.

640 Based on the ~~now included first exemplary initial~~ datasets within TephAta, several data-specific conclusions can be drawn. The integrity of sample and site metadata and descriptions ~~reveals~~ ~~reveal~~ that field notes and laboratory documentation are currently recorded at different levels of detail and often lacks crucial information, probably because the samples were not collected from a tephrostratigraphic perspective. The structure given in TephAta, in combination with specific field support (sample report templates, app-based field logs such as StraboSpot) will simplify and foster better documentation and archiving of data in the future and will facilitate public reporting of analytical details ~~that adhere to the tephra community best practice metadata.~~

In this study, tephra layers have predominantly rhyolitic glass compositions. The geochemical characterization of the studied tephra layers reveals a mostly rhyolitic composition. While major and minor element glass compositions can differentiate only some tephra layers, trace element glass compositions provide most robust means of distinction. Major and minor element glass composition can only be used to distinguish between some of the tephra layers. The majority of tephra layers can rather be distinguished based on their trace element glass compositions. Based on these observed geochemical differences, at least 16 different eruptive events can be distinguished have been identified, allowing for and potential regional correlations proposed.

Besides these achievements, the significant uncertainties in current geochronological data necessitate careful review. Existing ages should be supplemented by additional ages of more precise dating methods, before used as tephrochronological tie points. Besides these achievements, the large uncertainties of their chronological information suggest that existing ages must be carefully reviewed and supplemented, e.g., by additional ages of more confined dating methods, before used as tephrochronological tie points. Applying alternative/Implementing dating methods such as zircon double-dating (Danišik et al., 2017), will help to account for to exclude the influence of pre-eruptive mineral histories of dated minerals, will allow and to further assess tephra layers with similar age and geochemistry. Furthermore, Obtaining new chronological information data for this is also of interest for the numerous identified eruptive events (CG1-1, 4-8, 10, 11, 13-16), is essential to strengthen the tephrochronological framework for which no chronological information is available at present. This will support the growing tephrostratigraphic framework and will facilitate ensure the transfer of ages to sedimentary archives and thus help to overcome/overcoming the inherent dating challenges of the desert environment.dating issues of desert sediments.

Overall, this first set of initial dataset samples demonstrates already illustrates the potential and usefulness of a tephrostratigraphic and tephrochronological database for the region. However, The study also indicates-highlights that the development of a regional tephrostratigraphic-tephrochronological framework requires a substantial sample set with sufficient spatial and temporal coverage. This includes the tephrochronological characterization of proximal major eruptive products to link the -identified widespread tephra layers with their volcanic sources. A-As it expands, the database will deepen our understanding of the Andean volcanic history, where distal archives play a critical role in disentangling eruptive sequences, as demonstrated in other regions.growing database will also contribute to a better understanding of the volcanic history of the Andes. For example, distal archives have been proven to play an important role in disentangling explosive volcanic eruptive histories (Schindlbeck et al., 2018; Leicher et al., 2023; Vineberg et al., 2024). In addition, the individual geochemical data of tephra samples provides the opportunity to study magmatic processes, such as the varying degrees of element depletion/enrichment of characteristic elements observed in this dataset,such as indicated by the different degree of depletion/enrichment of characteristic elements in the presented dataset.

680 Supplement:

Supplementary Material

Overview of input masks for the seven different categories (Site, Sample, Physical Properties, Geochemistry, Chronology, Chronostratigraphy, Tephra Correlation Group) of the TephAta database are displayed below. A list of all input fields and their brief description is given in Supplementary Table 1. A list of all dropdown options is given in Supplementary Table 2.

685

Supplementary Table 1:

Overview table of input fields within TephAtaTA. For each input option within TephAta, the respective field name is given along with its overall category (e.g., “site” or “geochemistry”), the field type (e.g., text, dropdown selection, or data upload) and a short explanation of the respective field.

690

Supplementary Table 2:

-The table contains all dropdown options within the TephAta database, organized by their respective categories and input fields.

695 **Author contribution**

Conceptualization: NL, VW, BW, GB

Data curation: NL, VF

Funding acquisition, Supervision: VW, BW, GB

Resources: AQJ, PVI, FSV, GG, CB, AS, DG, LC, IRA

700 Software: VF, TK,

Investigation, Validation, Methodology: NL, VW, FW, ML, KK

Writing (original draft preparation), Visualization: NL

Writing (review and editing): all authors

705 **Competing interests:** The authors declare that they have no conflict of interest.

Acknowledgement

This research has been supported by the German Research Foundation (DFG) as part of Collaborative Research Centre (CRC) 1211 “Earth – Evolution at the Dry Limit”, sub-project D06, A02 and Z03 (grant nos. SFB 1211/2 2020. SFB1211/3 2024).

710 AQ, PV, FS received funding of the National Mapping Program of the SERNAGEOMIN. Gerhard Wörner, Jay Quade, Theresa Jordan, Felipe Aguilera Barraza, and Susana Layana are gratefully acknowledged for sharing sample material. Chong, G., and Jensen A. (Universidad Católica del Norte, Antofagasta) supported AS and LC during sampling. Furthermore, all (associated) CRC members who contributed sample material or assisted during field work are recognized. Reiner Kleinschrodt, Yannick Busweiler and Hanna Cieszynski are thanked for providing access to and supporting the use of the EPMA-WDS and SEM-EDS at the University of Cologne.

References

, !!! INVALID CITATION !!! (Tomlinson et al., 2012b; Pearce, 2014; Hopkins et al., 2021).

720 Abbott, P. M., Griggs, A. J., Bourne, A. J., Chapman, M. R., and Davies, S. M.: Tracing marine cryptotephra in the North Atlantic during the last glacial period: Improving the North Atlantic marine tephrostratigraphic framework, *Quat. Sci. Rev.*, 189, 169-186, <https://doi.org/10.1016/j.quascirev.2018.03.023>, 2018.

725 Albert, P. G., Smith, V. C., Suzuki, T., McLean, D., Tomlinson, E. L., Miyabuchi, Y., Kitaba, I., Mark, D. F., Moriwaki, H., Nakagawa, T., and Members, S. P.: Geochemical characterisation of the Late Quaternary widespread Japanese tephrostratigraphic markers and correlations to the Lake Suigetsu sedimentary archive (SG06 core), *Quat. Geochronol.*, 52, 103-131, <https://doi.org/10.1016/j.quageo.2019.01.005>, 2019.

Allmendinger, R. W., Jordan, T. E., Kay, S. M., and Isacks, B. L.: The evolution of the Altiplano-Puna plateau of the Central Andes, *Annu. Rev. Earth Planet. Sci.*, 25, 139-174, <https://doi.org/10.1146/annurev.earth.25.1.139>, 1997.

730 Astudillo, N., Ferrando, R., Montecino, D., Espinoza, F., Venegas, C., Matthews, S., Cornejo, P., and Arévalo, C.: Carta Augusta Victoria, región de Antofagasta, Servicio Nacional de Geología y Minería, Carta Geológica de Chile, Serie Geología Básica, 189, Santiago, Chile, 97 p., ISSN:0717-7283 Inscripción No. 285.185, 2017.

735 Blanco, N. and Tomlinson, A.: Carta Guatacondo, región de Tarapacá, Servicio Nacional de Geología y Minería, Carta Geológica de Chile, Serie Geología Básica, 156, Santiago, Chile, 116 p., ISSN:0717-7283 Inscripción No. 235.690, 2013.

Brandmeier, M. and Wörner, G.: Compositional variations of ignimbrite magmas in the Central Andes over the past 26 Ma — A multivariate statistical perspective, *Lithos*, 262, 713-728, <https://doi.org/10.1016/j.lithos.2016.07.011>, 2016.

740 Breitzkreuz, C., de Silva, S. L., Wilke, H. G., Pfänder, J. A., and Renno, A. D.: Neogene to Quaternary ash deposits in the Coastal Cordillera in northern Chile: Distal ashes from supereruptions in the Central Andes, *J. Volcanol. Geotherm. Res.*, 269, 68-82, <https://doi.org/10.1016/j.jvolgeores.2013.11.001>, 2014.

- 745 Bronk Ramsey, C., Housley, R. A., Lane, C. S., Smith, V. C., and Pollard, A. M.: The RESET tephra database and associated analytical tools, *Quat. Sci. Rev.*, 118, 33-47, <https://doi.org/10.1016/j.quascirev.2014.11.008>, 2015.
- Burns, D. H. and de Silva, S. L.: Andesites and evolution of the continental crust: Perspectives from the Central Volcanic Zone of the Andes, *Front. Earth Sci.*, 10, <https://doi.org/10.3389/feart.2022.961130>, 2023.
- 750 Burns, D. H., de Silva, S. L., Tepley, F., Schmitt, A. K., and Loewen, M. W.: Recording the transition from flare-up to steady-state arc magmatism at the Purico-Chascon volcanic complex, northern Chile, *Earth Planet. Sci. Lett.*, 422, 75-86, <https://doi.org/10.1016/j.epsl.2015.04.002>, 2015.
- 755 Cameron, C. E., Crass, S. W., and Staff, A.: Geologic database of information on volcanoes in Alaska (GeoDIVA), DDS, 20, <https://doi.org/10.14509/30901>, 2022.
- Carrizo, D., González, G., and Dunai, T.: Constricción neógena en la Cordillera de la Costa, norte de Chile: neotectónica y datación de superficies con ^{21}Ne cosmogónico, *Rev. Geol. Chile*, 35, 01-38, <http://dx.doi.org/10.4067/S0716-02082008000100001>, 2008.
- 760 CRC1211DB-TephATA: <https://www.crc1211db.uni-koeln.de/tephata/>, last access: 16 March 2026.
- Danišík, M., Schmitt, A. K., Stockli, D. F., Lovera, O. M., Dunkl, I., and Evans, N. J.: Application of combined U-Th-disequilibrium/U-Pb and (U-Th)/He zircon dating to tephrochronology, *Quat. Geochronol.*, 40, 23-32, <https://doi.org/10.1016/j.quageo.2016.07.005>, 2017.
- 765 de Silva, S. L.: Altiplano-Puna volcanic complex of the central Andes, *Geology*, 17, 1102-1106, [https://doi.org/10.1130/0091-7613\(1989\)017%3C1102:APVCOT%3E2.3.CO;2](https://doi.org/10.1130/0091-7613(1989)017%3C1102:APVCOT%3E2.3.CO;2), 1989a.
- de Silva, S. L.: Geochronology and stratigraphy of the ignimbrites from the $21^{\circ}30'S$ to $23^{\circ}30'S$ portion of the Central Andes of northern Chile, *J. Volcanol. Geotherm. Res.*, 37, 93-131, [https://doi.org/10.1016/0377-0273\(89\)90065-6](https://doi.org/10.1016/0377-0273(89)90065-6), 1989b.
- 770 de Silva, S. L. and Kay, S. M.: Turning up the Heat: High-Flux Magmatism in the Central Andes, *Elements*, 14, 245-250, <https://doi.org/10.2138/gselements.14.4.245>, 2018.
- 775 Dunai, T. J., González López, G. A., and Juez-Larré, J.: Oligocene-Miocene age of aridity in the Atacama Desert revealed by exposure dating of erosion-sensitive landforms, *Geology*, 33, 321-324, <https://doi.org/10.1130/G21184.1>, 2005.
- Dunai, T. J., Melles, M., Quandt, D., Knief, C., and Amelung, W.: Whitepaper: Earth – Evolution at the dry limit, *Global Planet. Change*, 193, 103275, <https://doi.org/10.1016/j.gloplacha.2020.103275>, 2020.
- 780 Escribano, A., Martínez, E., Domagala, J. P., Padel, M., Espinoza, V., Jorquera, B., Contreras, F., Pablo, J., De La Cruz, S., and Calderón, N.: Cartas Bahía Isla Blanca y Taltal, región de Antofagasta Servicio Nacional de Geología y Minería, Carta Geológica de Chile, Serie Geología Básica 164-165, Santiago, Chile, 75 p., ISSN:0717-7283 Inscripción No. 235.124, 2013.
- 785 Evenstar, L. A., Mather, A. E., Hartley, A. J., Stuart, F. M., Sparks, R. S. J., and Cooper, F. J.: Geomorphology on geologic timescales: Evolution of the late Cenozoic Pacific paleosurface in Northern Chile and Southern Peru, *Earth Sci. Rev.*, 171, 1-27, <https://doi.org/10.1016/j.earscirev.2017.04.004>, 2017.
- 790 Feng, W., Yang, J., Bao, C., Kong, D., and Chen, M.-T.: A Millennial-Scale Tephra Event-Stratigraphic Record of the South China Sea since the Penultimate Interglacial, *Lithosphere*, 2022, <https://doi.org/10.2113/2022/9074201>, 2022.
- Fornari, M., Risacher, F., and Féraud, G.: Dating of paleolakes in the central Altiplano of Bolivia, *Palaeogeogr. Palaeoclimatol. Palaeoecol.*, 172, 269-282, [https://doi.org/10.1016/S0031-0182\(01\)00301-7](https://doi.org/10.1016/S0031-0182(01)00301-7), 2001.
- 795 Fritz, S. C., Baker, P. A., Lowenstein, T. K., Seltzer, G. O., Rigsby, C. A., Dwyer, G. S., Tapia, P. M., Arnold, K. K., Ku, T. L., and Luo, S. D.: Hydrologic variation during the last 170,000 years in the southern hemisphere tropics of South America, *Quat. Res.*, 61, 95-104, <https://doi.org/10.1016/j.yqres.2003.08.007>, 2004.
- 800 Gardeweg, M. and Sellés, D.: Geología del área Collacagua-Rinconada, región de Tarapacá, Servicio Nacional de Geología y Minería, Carta Geológica de Chile, Serie Geología Básica Santiago, Chile, 84 p., ISSN:0717-7283 Inscripción No. 235.793, 2013.
- Gehrels, M. J., Lowe, D. J., Hazell, Z. J., and Newnham, R. M.: A continuous 5300-yr Holocene cryptotephrostratigraphic record from northern New Zealand and implications for tephrochronology and volcanic hazard assessment, *The Holocene*, 16, 173-187, <https://doi.org/10.1191/0959683606hl918rp>, 2006.
- 805 Giaccio, B., Leicher, N., Mannella, G., Monaco, L., Regattieri, E., Wagner, B., Zanchetta, G., Gaeta, M., Marra, F., Nomade, S., Palladino, D. M., Pereira, A., Scheidt, S., Sottili, G., Wonik, T., Wulf, S., Zeeden, C., Ariztegui, D., Cavinato, G. P., Dean, J. R., Florindo, F., Leng, M. J., Macri, P., Niespolo, E., Renne, P. R., Rolf, C., Sadori, L., Thomas, C., and Tzedakis, P. C.: Extending the tephra and palaeoenvironmental record of the Central Mediterranean back to 430 ka: A new core from Fucino Basin, central Italy, *Quat. Sci. Rev.*, 225, 106003, <https://doi.org/10.1016/j.quascirev.2019.106003>, 2019.
- 810 Griggs, A. J., Davies, S. M., Abbott, P. M., Rasmussen, T. L., and Palmer, A. P.: Optimising the use of marine tephrochronology in the North Atlantic: a detailed investigation of the Faroe Marine Ash Zones II, III and IV, *Quat. Sci. Rev.*, 106, 122-139, <https://doi.org/10.1016/j.quascirev.2014.04.031>, 2014.

- 815 Hopkins, J. L., Bidmead, J. E., Lowe, D. J., Wysoczanski, R. J., Pillans, B. J., Ashworth, L., Rees, A. B. H., and Tuckett, F.: TephraNZ: a major- and trace-element reference dataset for glass-shard analyses from prominent Quaternary rhyolitic tephros in New Zealand and implications for correlation, *GChron*, 3, 465-504, <https://doi.org/10.5194/gchron-3-465-2021>, 2021.
- 820 Hora, J. M., Singer, B. S., Jicha, B. R., Beard, B. L., Johnson, C. M., de Silva, S., and Salisbury, M.: Volcanic biotite-sanidine $^{40}\text{Ar}/^{39}\text{Ar}$ age discordances reflect Ar partitioning and pre-eruption closure in biotite, *Geology*, 38, 923-926, <https://doi.org/10.1130/g31064.1>, 2010.
- Horn, S.: Intra- und intervulkanische Variationen entlang der Zentralen Vulkanzone in Nordchile (17-22 °S): · Petrographische und geochemische Untersuchungen, Diploma thesis, Institut für Geowissenschaften, Johannes Gutenberg Universität Mainz, Mainz, 168 pp., 1991.
- 825 Jochum, K. P., Weis, U., Stoll, B., Kuzmin, D., Yang, Q. C., Raczek, I., Jacob, D. E., Stracke, A., Birbaum, K., Frick, D. A., Gunther, D., and Enzweiler, J.: Determination of Reference Values for NIST SRM 610-617 Glasses Following ISO Guidelines, *Geostand. Geoanal. Res.*, 35, 397-429, <https://doi.org/10.1111/j.1751-908X.2011.00120.x>, 2011.
- 830 Jochum, K. P., Stoll, B., Herwig, K., Willbold, M., Hofmann, A. W., Amini, M., Aarburg, S., Abouchami, W., Hellebrand, E., Mocek, B., Raczek, I., Stracke, A., Alard, O., Bouman, C., Becker, S., Ducking, M., Bratz, H., Klemd, R., de Bruin, D., Canil, D., Cornell, D., de Hoog, C. J., Dalpe, C., Danyushevsky, L., Eisenhauer, A., Gao, Y. J., Snow, J. E., Goschopf, N., Gunther, D., Latkoczy, C., Guillong, M., Hauri, E. H., Hofer, H. E., Lahaye, Y., Horz, K., Jacob, D. E., Kasemann, S. A., Kent, A. J. R., Ludwig, T., Zack, T., Mason, P. R. D., Meixner, A., Rosner, M., Misawa, K. J., Nash, B. P., Pfander, J., Premo, W. R., Sun, W. D., Tiepolo, M., Vannucci, R., Vennemann, T., Wayne, D., and Woodhead, J. D.: MPI-DING reference glasses for in situ microanalysis: New reference values for element concentrations and isotope ratios, *Geochem. Geophys. Geosyst.*, 7, 1525-2027, <https://doi.org/10.1029/2005gc001060>, 2006.
- 835 Jordan, T. E., Kirk-Lawlor, N. E., Blanco, N., Rech, J. A., and Cosentino, N. J.: Landscape modification in response to repeated onset of hyperarid paleoclimate states since 14 Ma, Atacama Desert, Chile, *Geol. Soc. Am. Bull.*, 126, 1016-1046, <https://doi.org/10.1130/B30978.1>, 2014.
- Kay, S. M., Coira, B. L., Caffè, P. J., and Chen, C. H.: Regional chemical diversity, crustal and mantle sources and evolution of central Andean Puna plateau ignimbrites, *J. Volcanol. Geotherm. Res.*, 198, 81-111, <https://doi.org/10.1016/j.jvolgeores.2010.08.013>, 2010.
- 845 Kern, J. M., de Silva, S. L., Schmitt, A. K., Kaiser, J. F., Iriarte, A. R., and Economos, R.: Geochronological imaging of an episodically constructed subvolcanic batholith: U-Pb in zircon chronochemistry of the Altiplano-Puna Volcanic Complex of the Central Andes, *Geosphere*, 12, 1054-1077, <https://doi.org/10.1130/ges01258.1>, 2016.
- 850 Kirk-Lawlor, N. E., Jordan, T. E., Rech, J. A., and Lehmann, S. B.: Late Miocene to Early Pliocene paleohydrology and landscape evolution of Northern Chile, 19° to 20° S, *Palaeogeogr. Palaeoclimatol. Palaeoecol.*, 387, 76-90, <https://doi.org/10.1016/j.palaeo.2013.07.011>, 2013.
- Koppers, A. A. P.: ArArCALC—software for $^{40}\text{Ar}/^{39}\text{Ar}$ age calculations, *Comput. Geosci.*, 28, 605-619, [https://doi.org/10.1016/S0098-3004\(01\)00095-4](https://doi.org/10.1016/S0098-3004(01)00095-4), 2002.
- 855 Kuehn, S., Bursik, M., Kurbatov, A., Lehnert, K., Loewen, M., Profeta, L., Ramdeen, S., and Wallace, K.: Tephra Community Tools for Archiving Sample Information, Analytical Methods, Samples Geochemistry, and Standards Geochemistry at SESAR and EarthChem, *Microsc. Microanal.*, 29, 242-242, <https://doi.org/10.1093/micmic/ozad067.108>, 2023.
- 860 Kuiper, K. F., Deino, A., Hilgen, F. J., Krijgsman, W., Renne, P. R., and Wijbrans, J. R.: Synchronizing Rock Clocks of Earth History, *Science*, 320, 500-504, <https://doi.org/10.1126/science.1154339>, 2008.
- Kurbatov, A., Dunbar, N. W., Iverson, N. A., Gerbi, C. C., Yates, M. G., Kalteyer, D., and McIntosh, W. C.: Antarctic Tephra Database (AntT) AGU Fall Meeting 2014, San Francisco, 15-19 December 2014, V31C-4760, 2014.
- 865 Kutterolf, S., Schindlbeck, J. C., Anselmetti, F. S., Ariztegui, D., Brenner, M., Curtis, J., Schmid, D., Hodell, D. A., Mueller, A., Pérez, L., Pérez, W., Schwalb, A., Frische, M., and Wang, K. L.: A 400-ka tephrochronological framework for Central America from Lake Petén Itzá (Guatemala) sediments, *Quat. Sci. Rev.*, 150, 200-220, <https://doi.org/10.1016/j.quascirev.2016.08.023>, 2016.
- 870 Le Bas, M. J. L., Maitre, R. W. L., Streckeisen, A., and Zanettin, B.: A Chemical Classification of Volcanic Rocks Based on the Total Alkali-Silica Diagram, *J. Petrol.*, 27, 745-750, <https://doi.org/10.1093/petrology/27.3.745>, 1986.
- Lee, J. Y., Marti, K., Severinghaus, J. P., Kawamura, K., Yoo, H. S., Lee, J. B., and Kim, J. S.: A redetermination of the isotopic abundances of atmospheric Ar, *Geochim. Cosmochim. Acta*, 70, 4507-4512, <https://doi.org/10.1016/j.gca.2006.06.1563>, 2006.
- 875 Leicher, N.: EPMA-WDS settings for glass at University of Cologne - v1, Interdisciplinary Earth Data Alliance (IEDA) [dataset], <https://doi.org/10.26022/IEDA/111986>, 2021.
- Leicher, N. and Lagos, M.: LA-ICP-MS at University of Bonn - v1, Interdisciplinary Earth Data Alliance (IEDA) [dataset], <https://doi.org/10.26022/IEDA/111989>, 2021.
- 880 Leicher, N., Giaccio, B., Zanchetta, G., Sulpizio, R., Albert, P. G., Tomlinson, E. L., Lagos, M., Francke, A., and Wagner, B.: Lake Ohrid's tephrochronological dataset reveals 1.36 Ma of Mediterranean explosive volcanic activity, *Sci. Data*, 8, 231, <https://doi.org/10.1038/s41597-021-01013-7>, 2021.

- 885 Leicher, N., Monaco, L., Giaccio, B., Nomade, S., Pereira, A., Mannella, G., Wulf, S., Sottili, G., Palladino, D. M., Zanchetta, G., and Wagner, B.: Central Mediterranean tephrochronology for the time interval 250–315 ka derived from the Fucino sediment succession, *Boreas*, 53, 164-185, <https://doi.org/10.1111/bor.12637>, 2023.
- 890 Leicher N., W. V., Wombacher F., Lagos, M.: Tephrostratigraphic and tephrochronological dataset of tephra layers from northern Chile, Version 1.0, Interdisciplinary Earth Data Alliance (IEDA) [dataset], <https://doi.org/10.60520/IEDA/114209>, 2026.
- Lowe, D. J.: Tephrochronology and its application: A review, *Quat. Geochronol.*, 6, 107-153, <https://doi.org/10.1016/j.quageo.2010.08.003>, 2011.
- 895 Lowe, D. J., Blaauw, M., Hogg, A. G., and Newnham, R. M.: Ages of 24 widespread tephra erupted since 30,000 years ago in New Zealand, with re-evaluation of the timing and palaeoclimatic implications of the Lateglacial cool episode recorded at Kaipo bog, *Quat. Sci. Rev.*, 74, 170-194, <https://doi.org/10.1016/j.quascirev.2012.11.022>, 2013.
- 900 Lowe, D. J., Pearce, N. J. G., Jorgensen, M. A., Kuehn, S. C., Tryon, C. A., and Hayward, C. L.: Correlating tephra and cryptotephra using glass compositional analyses and numerical and statistical methods: Review and evaluation, *Quat. Sci. Rev.*, 175, 1-44, <https://doi.org/10.1016/j.quascirev.2017.08.003>, 2017.
- 905 Lowe, J. J., Ramsey, C. B., Housley, R. A., Lane, C. S., and Tomlinson, E. L.: The RESET project: constructing a European tephra lattice for refined synchronisation of environmental and archaeological events during the last c. 100 ka, *Quat. Sci. Rev.*, 118, 1-17, <https://doi.org/10.1016/j.quascirev.2015.04.006>, 2015.
- Mamani, M., Wörner, G., and Sempere, T.: Geochemical variations in igneous rocks of the Central Andean orocline (13°S to 18°S): Tracing crustal thickening and magma generation through time and space, *Geol. Soc. Am. Bull.*, 122, 162-182, <https://doi.org/10.1130/B26538.1>, 2010.
- 910 Mana, S. and DiMaggio, E.: Broadening Access To Volcanic Datasets From East Africa, Connects 2023, Pittsburgh, Pennsylvania, USA, 15-18 October 2023, 2023AM-393916, <https://doi.org/10.1130/abs/2023AM-393916>, 2023.
- 915 Marinovic, N., Smoje, I., Maksić, V., Herve, M., and Mpodozis, C.: Hoja Aguas Blancas, Servicio Nacional de Geología y Minería, Carta Geológica de Chile, Serie Geología Básica 70, Santiago, Chile, 150 p., ISSN:0716-7555 Inscripción No. 81271, 1995.
- 920 Marquardt, C., Fornari, M., Lavenu, A., Easton, G., Ortlieb, L., Ritz, J.-F., and Philip, H.: Volcanic ash dating from the Mejillones Peninsula (23°S): Implications for the Neogene outer fore-arc stratigraphy, tectonics and volcanic relationships, 6th International Symposium on Andean Geodynamics, Barcelona, 12-14 September 2005, Extended Abstracts: 477-480, 2005.
- Martínez Fontaine, C., Peña-Araya, V., Marmo, C., Le Morvan, M., Delpech, G., Fontijn, K., Siani, G., and Cosyn-Wexsteen, L.: BOOM! Tephrochronological dataset and exploration tool of the Southern (33–46° S) and Austral (49–55° S) volcanic zones of the Andes, *Quat. Sci. Rev.*, 316, 108254, <https://doi.org/10.1016/j.quascirev.2023.108254>, 2023.
- 925 May, S. M., Meine, L., Hoffmeister, D., Brill, D., Medialdea, A., Wennrich, V., Gröbner, M., Schulte, P., Steininger, F., Deprez, M., de Kock, T., and Bubbenzer, O.: Origin and timing of past hillslope activity in the hyper-arid core of the Atacama Desert – The formation of fine sediment lobes along the Chuculay Fault System, Northern Chile, *Global Planet. Change*, 184, 103057, <https://doi.org/10.1016/j.gloplacha.2019.103057>, 2020.
- 930 McDonough, W. F. and Sun, S. S.: The composition of the Earth, *Chem. Geol.*, 120, 223-253, [https://doi.org/10.1016/0009-2541\(94\)00140-4](https://doi.org/10.1016/0009-2541(94)00140-4), 1995.
- 935 Medialdea, A., May, S. M., Brill, D., King, G., Ritter, B., Wennrich, V., Bartz, M., Zander, A., Kuiper, K., Hurtado, S., Hoffmeister, D., Schulte, P., Gröbner, M., Opitz, S., Brückner, H., and Bubbenzer, O.: Identification of humid periods in the Atacama Desert through hillslope activity established by infrared stimulated luminescence (IRSL) dating, *Global Planet. Change*, 185, 103086, <https://doi.org/10.1016/j.gloplacha.2019.103086>, 2020.
- 940 Medina, E., Jensen, A., Niemeyer, H., Wilke, H. G., Cembrano, J., García, M., Riquelme, R., Espinoza, S., and Chong, G.: Cartas Tocopilla y Maria Elena, región de Antofagasta, Servicio Nacional de Geología y Minería, Carta Geológica de Chile, Serie Geología Básica, 141-142, Santiago, Chile, 58 p., ISSN:0717-7283 Inscripción No. 224.403, 2012.
- Mín, K., Mundil, R., Renne, P. R., and Ludwig, K. R.: A test for systematic errors in ⁴⁰Ar/³⁹Ar geochronology through comparison with U/Pb analysis of a 1.1-Ga rhyolite, *Geochim. Cosmochim. Acta*, 64, 73-98, [https://doi.org/10.1016/S0016-7037\(99\)00204-5](https://doi.org/10.1016/S0016-7037(99)00204-5), 2000.
- 945 Newton, A. J., Dugmore, A. J., and Gittings, B. M.: Tephrobase: tephrochronology and the development of a centralised European database, *J. Quat. Sci.*, 22, 737-743, <https://doi.org/10.1002/jqs.1094>, 2007.
- 950 Oliveros, V., González, J., Espinoza Vargas, M., Vásquez, P., Rossel, P., Creixell, C., Sepúlveda, F., and Bastias, F.: The Early Stages of the Magmatic Arc in the Southern Central Andes, in: *The Evolution of the Chilean-Argentinean Andes*, edited by: Folguera, A., Contreras-Reyes, E., Heredia, N., Encinas, A., B. Iannelli, S., Oliveros, V., M. Dávila, F., Collo, G., Giambiagi, L., Maksymowicz, A., Iglesia Llanos, M. P., Turienzo, M., Naipauer, M., Orts, D., D. Litvak, V., Alvarez, O., and Arriagada, C., Springer International Publishing, Cham, 165-190, https://doi.org/10.1007/978-3-319-67774-3_7, 2018.
- 955 Paton, C., Hellstrom, J., Paul, B., Woodhead, J., and Hergt, J.: Iolite: Freeware for the visualisation and processing of mass spectrometric data, *J. Anal. At. Spectrom.*, 26, 2508-2518, <https://doi.org/10.1039/c1ja10172b>, 2011.

- Pearce, N. J. G.: Towards a protocol for the trace element analysis of glass from rhyolitic shards in tephra deposits by laser ablation ICP-MS, *J. Quat. Sci.*, 29, 627-640, <https://doi.org/10.1002/jqs.2727>, 2014.
- 960 Phillips, D. and Matchan, E. L.: Ultra-high precision $^{40}\text{Ar}/^{39}\text{Ar}$ ages for Fish Canyon Tuff and Alder Creek Rhyolite sanidine: New dating standards required?, *Geochim. Cosmochim. Acta*, 121, 229-239, <https://doi.org/10.1016/j.gca.2013.07.003>, 2013.
- Placzek, C., Quade, J., Rech, J. A., Patchett, P. J., and de Arce, C. P.: Geochemistry, chronology and stratigraphy of Neogene tuffs of the Central Andean region, *Quat. Geochronol.*, 4, 22-36, <https://doi.org/10.1016/j.quageo.2008.06.002>, 2009.
- 965 Portnyagin, M. V., Ponomareva, V. V., Zelenin, E. A., Bazanova, L. I., Pevzner, M. M., Plechova, A. A., Rogozin, A. N., and Garbe-Schönberg, D.: TephraKam: geochemical database of glass compositions in tephra and welded tuffs from the Kamchatka volcanic arc (northwestern Pacific), *Earth Syst. Sci. Data*, 12, 469-486, <https://doi.org/10.5194/essd-12-469-2020>, 2020.
- 970 Quezada, A., Blanco, N., Vásquez, P., and Sepúlveda, F.: Ar-Ar (biotite) dating of deformed tephra layers (ashes) interbedded in salar Grande halite deposits, Atacama Desert, I Region, Chile, 15. Congreso Geológico Chileno, Cocepción, Chile, 18-23 November 2018, 15785-a, 2018.
- Riede, F., Bazely, O., Newton, A. J., and Lane, C. S.: A Laacher See-eruption supplement to Tephabase: Investigating distal tephra fallout dynamics, *Quat. Int.*, 246, 134-144, <https://doi.org/10.1016/j.quaint.2011.06.029>, 2011.
- 975 Ritter, B., Stuart, F. M., Binnie, S. A., Gerdes, A., Wennrich, V., and Dunai, T. J.: Neogene fluvial landscape evolution in the hyperarid core of the Atacama Desert, *Sci. Rep.*, 8, 13952, <https://doi.org/10.1038/s41598-018-32339-9>, 2018.
- 980 Ritter, B., Diederich-Leicher, J. L., Binnie, S. A., Stuart, F. M., Wennrich, V., Bolten, A., and Dunai, T. J.: Impact of CaSO_4 -rich soil on Miocene surface preservation and Quaternary sinuous to meandering channel forms in the hyperarid Atacama Desert, *Sci. Rep.*, 12, 17951, <https://doi.org/10.1038/s41598-022-22787-9>, 2022.
- Ritter, B., Mohren, J., Binnie, S. A., Wennrich, V., Dunkl, I., Albert, R., Gerdes, A., LoBue, S., and Dunai, T. J.: Shaping the Huará Intrusive Complex in the Hyperarid Atacama Desert-Erosional Near-Stasis Contrasting High Topographic Gradients, *J. Geophys. Res.: Earth Surf.*, 128, e2022JF006986, <https://doi.org/10.1029/2022jf006986>, 2023.
- 985 Rodríguez, I., Roche, O., Moune, S., Aguilera, F., Campos, E., and Pizarro, M.: Evolution of Irruputuncu volcano, Central Andes, northern Chile, *J. South Am. Earth Sci.*, 63, 385-399, <https://doi.org/10.1016/j.jsames.2015.08.012>, 2015.
- 990 Sáez, A., Cabrera, L., Jensen, A., and Chong, G.: Late Neogene lacustrine record and palaeogeography in the Quillagua–Llamara basin, Central Andean fore-arc (northern Chile), *Palaeogeogr. Palaeoclimatol. Palaeoecol.*, 151, 5-37, [https://doi.org/10.1016/S0031-0182\(99\)00013-9](https://doi.org/10.1016/S0031-0182(99)00013-9), 1999.
- 995 Sáez, A., Cabrera, L., Garcés, M., van den Bogaard, P., Jensen, A., and Gimeno, D.: The stratigraphic record of changing hyperaridity in the Atacama desert over the last 10 Ma, *Earth Planet. Sci. Lett.*, 355, 32-38, <https://doi.org/10.1016/j.epsl.2012.08.029>, 2012.
- Sáez, A., Hernández, A., Pimentel, A., Andrade, M., Bao, R., Raposeiro, P. M., Gonçalves, V., Benavente, M., Pla-Rabes, S., Ramalho, R., and Giral, S.: Westerlies migrations and volcanic records over the past 4000 years from the Azores lacustrine sequences. Exploring correlations and impacts on Western Europe, *Global Planet. Change*, 246, 104698, <https://doi.org/10.1016/j.gloplacha.2025.104698>, 2025.
- 1000 Sagawa, T., Nagahashi, Y., Satoguchi, Y., Holbourn, A., Itaki, T., Gallagher, S. J., Saavedra-Pellitero, M., Ikehara, K., Irino, T., and Tada, R.: Integrated tephrostratigraphy and stable isotope stratigraphy in the Japan Sea and East China Sea using IODP Sites U1426, U1427, and U1429, Expedition 346 Asian Monsoon, *Prog. Earth Planet. Sci.*, 5, 18, <https://doi.org/10.1186/s40645-018-0168-7>, 2018.
- 1005 Salisbury, M. J., Jicha, B. R., de Silva, S. L., Singer, B. S., Jiménez, N. C., and Ort, M. H.: $^{40}\text{Ar}/^{39}\text{Ar}$ chronostratigraphy of Altiplano-Puna volcanic complex ignimbrites reveals the development of a major magmatic province, *Geol. Soc. Am. Bull.*, 123, 821-840, <https://doi.org/10.1130/B30280.1>, 2011.
- 1010 Schindlbeck, J. C., Kutterolf, S., Freundt, A., Eisele, S., Wang, K.-L., and Frische, M.: Miocene to Holocene Marine Tephrostratigraphy Offshore Northern Central America and Southern Mexico: Pulsed Activity of Known Volcanic Complexes, *Geochem. Geophys. Geosyst.*, 19, 4143-4173, <https://doi.org/10.1029/2018GC007832>, 2018.
- 1015 Sepúlveda, F., González, E., and Tomlinson, A. J.: Geología y estructura del cuadrángulo Quebrada Arcas, región de Antofagasta, Chile, Servicio Nacional de Geología y Minería, Informe Registrado, IR-23-108, Santiago, Chile, 53 p., - Inscripción No. 2023-A-11832, 2023.
- Sepúlveda, F., Vásquez, P., and Quezada, A.: Geochronological record of Cenozoic pyroclastic eruptive events, Coastal Range of northern Chile (20° - 21° S), International Geological Congress on the Southern Hemisphere GEOSUR 2013, Viña del Mar, Chile, 25-27 November 2013, 199, 2013.
- 1020 Sepúlveda, F., Vásquez, P., and Quezada, A.: Cartas Patillos y Oficina Victoria, región de Tarapacá, Servicio Nacional de Geología y Minería, Carta Geológica de Chile, Serie Geología Básica, 167-168, Santiago, Chile, 107 p., ISSN:0717-7283 Inscripción No. 248.599, 2014.
- 1025 Sulpizio, R., Zanchetta, G., Paterne, M., and Siani, G.: A review of tephrostratigraphy in central and southern Italy during the last 65 ka, *Il Quaternario Italian Journal of Quaternary Sciences*, 16, 91-108, -, 2003.

- 1030 Tapia, C. A., Wilson, G. S., Ishman, S. E., Wilke, H. G., Wartho, J. A., Winter, D., and Martínez-Pardo, R.: An integrated sequence stratigraphic and chronostratigraphic analysis of the Pliocene, Tiburon Basin succession, Mejillones Peninsula, Chile, *Global Planet. Change*, 131, 124-147, <https://doi.org/10.1016/j.gloplacha.2015.05.005>, 2015.
- 1035 Tomlinson, E. L., Kinvig, H. S., Smith, V. C., Blundy, J. D., Gottsmann, J., Müller, W., and Menzies, M. A.: The Upper and Lower Nisyros Pumices: Revisions to the Mediterranean tephrostratigraphic record based on micron-beam glass geochemistry, *J. Volcanol. Geotherm. Res.*, 243, 69-80, <https://doi.org/10.1016/j.jvolgeores.2012.07.004>, 2012a.
- 1040 Tomlinson, E. L., Arienzo, I., Civetta, L., Wulf, S., Smith, V. C., Hardiman, M., Lane, C. S., Carandente, A., Orsi, G., Rosi, M., Müller, W., and Menzies, M. A.: Geochemistry of the Phlegraean Fields (Italy) proximal sources for major Mediterranean tephras: Implications for the dispersal of Plinian and co-ignimbritic components of explosive eruptions, *Geochim. Cosmochim. Acta*, 93, 102-128, <https://doi.org/10.1016/j.gca.2012.05.043>, 2012b.
- 1045 Vakhrameeva, P., Koutsodendris, A., Wulf, S., Portnyagin, M., Appelt, O., Ludwig, T., Trieloff, M., and Pross, J.: Land-sea correlations in the Eastern Mediterranean region over the past c. 800 kyr based on macro- and cryptotephras from ODP Site 964 (Ionian Basin), *Quat. Sci. Rev.*, 255, 106811, <https://doi.org/10.1016/j.quascirev.2021.106811>, 2021.
- 1050 van Zalinge, M. E., Sparks, R. S. J., Cooper, F. J., and Condon, D. J.: Early Miocene large-volume ignimbrites of the Oxaya Formation, Central Andes, *J. Geol. Soc.*, 173, 716-733, <https://doi.org/10.1144/jgs2015-123>, 2016.
- 1055 Vásquez, P. and Sepúlveda, F. A.: Cartas Iquique y Pozo Almonte, región de Tarapacá, Servicio Nacional de Geología y Minería, Carta Geológica de Chile, Serie Geología Básica, 162-163, Santiago, Chile, 114 p., ISSN:0717-7283 Inscripción No. 235.688, 2013.
- 1060 Vásquez, P., Sepúlveda, F., Quezada, A., Aguilef, S., Franco, C., and Blanco, N.: Cartas Guanillos del Norte y Salar de Llamara, regiones de Tarapacá y Antofagasta, Servicio Nacional de Geología y Minería, Carta Geológica de Chile, Carta Geológica de Chile, Serie Geología Básica, 195-196, Santiago, Chile, 93 p., ISSN:0717-7283 Inscripción No. 295.735, 2018.
- 1065 Vineberg, S. O., Albert, P. G., McLean, D., Suzuki, T., Staff, R. A., Yamada, K., Kitaba, I., Kitagawa, J., Manning, C. J., Buckland, H. M., Jones, G., Nishizawa, F., Nakagawa, T., and Smith, V. C.: A detailed record of large explosive eruptions from Japan between ~120 and 50 ka preserved at Lake Suigetsu, *Quat. Sci. Rev.*, 346, 109021, <https://doi.org/10.1016/j.quascirev.2024.109021>, 2024.
- 1070 Wallace, K. L., Bursik, M. I., Kuehn, S., Kurbatov, A. V., Abbott, P., Bonadonna, C., Cashman, K., Davies, S. M., Jensen, B., Lane, C., Plunkett, G., Smith, V. C., Tomlinson, E., Thordarsson, T., and Walker, J. D.: Community established best practice recommendations for tephra studies—from collection through analysis, *Sci. Data*, 9, 447, <https://doi.org/10.1038/s41597-022-01515-y>, 2022.
- 1065 Wennrich, V., Diederich-Leicher, J., Blanco-Arrué, B. N., Büttner, C., Buske, S., Sepulveda, E. C., Dunai, T., Feller, J., Galego, E., Hasberg, A., Leicher, N., López, D. A., Maldonado, J., Medialdea, A., Ninnemann, L., Perryman, R., Ríos-Contesse, J. C., Ritter, B., Scheidt, S., Vargas-Machuca, B., Yogeshwar, P., and Melles, M.: Unearthing the climate history of the Atacama Desert in northern Chile - deep drilling in two clay pans of the Coastal Cordillera, *Sci. Drill.*, 34, 1-20, <https://doi.org/10.5194/sd-34-1-2025>, 2025.
- 1070 Wilkinson, M. D., Dumontier, M., Aalbersberg, I. J., Appleton, G., Axton, M., Baak, A., Blomberg, N., Boiten, J.-W., da Silva Santos, L. B., Bourne, P. E., Bouwman, J., Brookes, A. J., Clark, T., Crosas, M., Dillo, I., Dumon, O., Edmunds, S., Evelo, C. T., Finkers, R., Gonzalez-Beltran, A., Gray, A. J. G., Groth, P., Goble, C., Grethe, J. S., Heringa, J., 't Hoen, P. A. C., Hooft, R., Kuhn, T., Kok, R., Kok, J., Lusher, S. J., Martone, M. E., Mons, A., Packer, A. L., Persson, B., Rocca-Serra, P., Roos, M., van Schaik, R., Sansone, S.-A., Schultes, E., Sengstag, T., Slater, T., Strawn, G., Swertz, M. A., Thompson, M., van der Lei, J., van Mulligen, E., Velterop, J., Waagmeester, A., Wittenburg, P., Wolstencroft, K., Zhao, J., and Mons, B.: The FAIR Guiding Principles for scientific data management and stewardship, *Sci. Data*, 3, 160018, <https://doi.org/10.1038/sdata.2016.18>, 2016.
- 1075 Wörner, G., Mamani, M., and Blum-Oeste, M.: Magmatism in the Central Andes, *Elements*, 14, 237-244, <https://doi.org/10.2138/gselements.14.4.237>, 2018.
- 1080 Wörner, G., Uhlig, D., Kohler, I., and Seyfried, H.: Evolution of the West Andean Escarpment at 18 S (N. Chile) during the last 25 Ma: uplift, erosion and collapse through time, *Tectonophysics*, 345, 183-198, [https://doi.org/10.1016/S0040-1951\(01\)00212-8](https://doi.org/10.1016/S0040-1951(01)00212-8), 2002.
- 1085 Wörner, G., Hammerschmidt, K., Henjes-Kunst, F., Lezaun, J., and Wilke, H.: Geochronology ($^{40}\text{Ar}/^{39}\text{Ar}$, K-Ar and He-exposure ages) of Cenozoic magmatic rocks from northern Chile (18-22 S): implications for magmatism and tectonic evolution of the central Andes, *Rev. Geol. Chile*, 27, 205-240, <http://dx.doi.org/10.4067/S0716-02082000000200004>, 2000.
- 1090 Wulf, S., Kraml, M., Brauer, A., Keller, J., and Negendank, J. F. W.: Tephrochronology of the 100 ka lacustrine sediment record of Lago Grande di Monticchio (Southern Italy), *Quat. Int.*, 122, 7-30, <https://doi.org/10.1016/j.quaint.2004.01.028>, 2004.